Received: 4 November 2021 | Revised: 22 December 2021 | Accepted: 5 January 2022

DOI: 10.1002/inf2.12299

REVIEW ARTICLE

WILEY

Structures, properties, and challenges of emerging 2D materials in bioelectronics and biosensors

Fan Chen[1] | Qing Tang[1] | Tian Ma[1] | Bihui Zhu[1] | Liyun Wang[1] | Chao He[1] | Xianglin Luo[1] | Sujiao Cao[1,2] | Lang Ma[1,2,3] | Chong Cheng[1]

[1]College of Polymer Science and Engineering, State Key Laboratory of Polymer Materials Engineering, Department of Ultrasound, West China Hospital, Med-X Center for Materials, Sichuan University, Chengdu, China

[2]National Clinical Research Center for Geriatrics, West China Hospital, Sichuan University, Chengdu, China

[3]Department of Chemistry and Biochemistry, Freie Universität Berlin, Berlin, Germany

Correspondence
Sujiao Cao, Lang Ma, and Chong Cheng, College of Polymer Science and Engineering, State Key Laboratory of Polymer Materials Engineering, Department of Ultrasound, West China Hospital, Med-X Center for Materials, Sichuan University, Chengdu 610065, China.
Email: caosujiao@scu.edu.cn, malang1989@scu.edu.cn and chong.cheng@scu.edu.cn

Funding information
1.3.5 Project for Disciplines of Excellence, West China Hospital, Sichuan University, Grant/Award Number: ZYJC21047; China Postdoctoral Science Foundation, Grant/Award Numbers: 2021M692291, 2021M692288, 2021M702334; Fundamental Research Funds for the Central Universities, Grant/Award Numbers: 2021SCU12034, 2021SCU12013; Med-X Center for Materials, Sichuan University, Grant/Award Number: MCM202102; National Natural Science Foundation of China, Grant/Award Numbers: 82001824, 82001829, 51903178, 81971622, 52173133, 82102064, 82102065, 82071938; Post-Doctor Research Project, West China Hospital, Sichuan University, Grant/Award Numbers: 2020HXBH071, 2020HXBH126; the National Key R D Program of China, Grant/Award

Abstract

Bioelectronics are powerful tools for monitoring and stimulating biological and biochemical processes, with applications ranging from neural interface simulation to biosensing. The increasing demand for bioelectronics has greatly promoted the development of new nanomaterials as detection platforms. Recently, owing to their ultrathin structures and excellent physicochemical properties, emerging two-dimensional (2D) materials have become one of the most researched areas in the fields of bioelectronics and biosensors. In this timely review, the physicochemical structures of the most representative emerging 2D materials and the design of their nanostructures for engineering high-performance bioelectronic and biosensing devices are presented. We focus on the structural optimization of emerging 2D material-based composites to achieve better regulation for enhancing the performance of bioelectronics. Subsequently, the recent developments of emerging 2D materials in bioelectronics, such as neural interface simulation, biomolecular/biomarker detection, and skin sensors are discussed thoroughly. Finally, we provide conclusive views on the current challenges and future perspectives on utilizing emerging 2D materials and their composites for bioelectronics and biosensors. This review will offer important guidance in designing and applying emerging 2D materials in bioelectronics, thus further promoting their prospects in a wide biomedical field.

KEYWORDS
bioelectronics, biosensors, emerging 2D materials, nanostructures and properties, neural interfaces simulation

Fan Chen and Qing Tang contributed equally to this study.

Numbers: 2021YFE0205000, 2019YFA0110600, 2019YFA0110601; the Science and Technology Project of Sichuan Province, Grant/Award Numbers: 2021YFH0087, 2021YFH0135, 2021YFS0050, 2021YFH0180, 2021YJ0434, 2021YJ0554, 21YYJC2714, 21ZDYF376; the Science and Technology Project of the Health Planning Committee of Sichuan, Grant/Award Number: 20PJ049; the State Key Laboratory of Polymer Materials Engineering, Grant/Award Number: sklpme2021-4-02; Thousand Youth Talents Plan

1 | INTRODUCTION

Bioelectronics is a fast-growing interdisciplinary field of research involving the integration of biomaterials with electronic transducers. Silicon-based electronics have been proven to apply to a wide range of biological and biochemical monitors and sensors, such as biochips, biosensors, and biophotoelectric imaging tubes.[1–6] However, silicon-based electronics face various challenges, including reduced carrier mobility, increased short-channel effects at sub-10 nm nodes, and limited flexibility. In particular, to promote flexibility, rigid silicon-based components are required to become ultra-thin, which is extremely difficult for device processing and reliable integration. In recent years, low-dimensional materials and their composites have been demonstrated to exhibit excellent physicochemical properties, such as electrical and optical properties, making them especially suitable for integration with low modulus to obtain high-performance electronic and photoelectric devices while withstanding large mechanical deformation.[7]

Since the discovery of graphene by Andre Geim and Konstantin Novoselov in 2004,[8,9] research on various properties and applications of two-dimensional (2D) materials are been conducted. Currently, 2D materials are defined as a single atomic plane, whereas 100 layers should be considered as three-dimensional (3D) thin films. To date, beyond graphene, emerging 2D materials, such as hexagonal boron nitride (*h*-BN),[10] graphitic carbon nitride (g-C_3N_4),[11] black phosphorus (BP),[12] metal and metal oxide nanosheets,[13] transition metal dichalcogenides (TMDs),[14] MXenes,[15] metal–organic frameworks (MOFs),[16] and covalent-organic frameworks (COFs),[17] have been widely studied and applied in biomedical fields. Moreover, from a material science point of view, owing to their intrinsic atomic thickness, mechanical flexibility, high transparency, high carrier transfer characteristics, and good biocompatibility at material-biological interfaces, the emerging 2D materials can not only address the requirements of bioelectronic devices but also skillfully avoiding the limitations of silicon-based electronic devices.[18–20] Together, they are promising for next-generation bioelectronics, such as flexible skin devices, neural interface sensors, electrode sequences, and field-effect devices.[21–25]

In addition, secondary engineering of emerging 2D materials and their composites, such as molecular tailoring and surface functionalization, is worth considering. Polymers are widely used for molecular tailoring because of their versatility and ease of synthesis.[26–29] Likewise, the emerging 2D materials with ultrathin structures or large surface areas make it convenient for surface decoration of versatile components, thus achieving multifunctional bioelectronics and biosensors applications. In addition to polymers and organic molecules,[30,31] emerging 2D materials also allow the loading of other functional nanomaterials, such as quantum dots,[32] silver nanoparticles,[33] and Fe_3O_4 nanoparticles,[34] thus resulting in a nanocomposite that integrates the performances from both sides. In general, the combination of emerging 2D materials with functional molecules/nanomaterials has boosted the development of solvent-processable nanodevices, physiologically stable and biocompatible monitoring nanoplatforms, and tissue/cell-adhesive nanointerfaces, which show promise for disease diagnosis, human body signal monitoring, and biosensing.

Considering the unlimited potential of emerging 2D materials in bioelectronics, it is assumed that with more insights into their structures and properties, their applications in bioelectronics/biosensors will be gradually expanded. In this review, the physicochemical structures of the most representative emerging 2D materials, such as g-C_3N_4, BP, TMDs, MXenes, metal/metal oxide nanosheets, 2D MOFs/COFs, and their composites, to engineer high-performance bioelectronic and biosensing devices are presented (Scheme 1). We focus on the

structural optimization of emerging 2D material-based composites to achieve better regulation for enhancing the performance of bioelectronics. Subsequently, the recent developments of emerging 2D materials in bioelectronics, such as neural interface simulation, biomolecular/biomarker detection, and skin sensors, have been introduced. Finally, we provide very conclusive views on the current challenges and future perspectives of utilizing emerging 2D materials and their composites for bioelectronics and biosensors.

2 | STRUCTURES, PROPERTIES, AND PERSPECTIVES OF EMERGING 2D MATERIALS FOR BIOELECTRONICS AND BIOSENSORS

Following the great success of graphene, emerging 2D materials beyond graphenes, such as g-C_3N_4, BP, TMDs, metal oxides, MXenes, and MOF/COF nanosheets, have garnered attention in the fields of materials science and

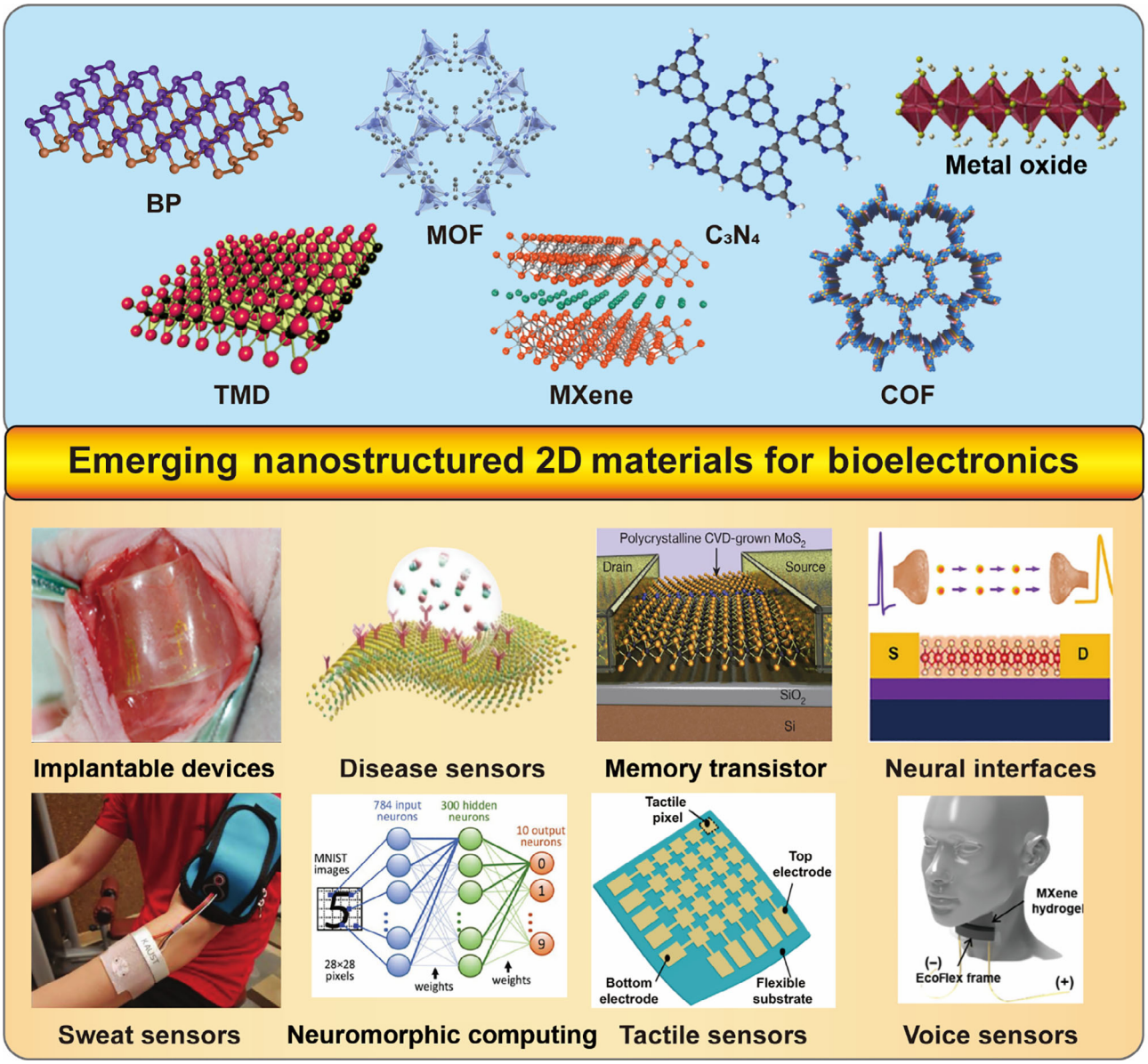

SCHEME 1 Illustration on the chemical structures of emerging 2D materials and their applications as bioelectronics and biosensors: Reproduced with permission.[35–42] Copyright 2017, Springer International Publishing AG. Copyright 2018, Nature Publishing Group. Copyright 2019, 2018, American Chemical Society. Copyright 2019, 2018, 2016, Wiley-VCH. Copyright 2018, American Association for the Advancement of Science. 2D, two-dimensional; BP, black phosphorus; COF, covalent-organic frameworks; CVD, chemical vapor deposition; MNIST, MOF, metal–organic frameworks; TMD, transition metal dichalcogenide

TABLE 1 Characteristics, applications, and performances of the emerging 2D material-based bioelectronic devices

		Characteristics	Bioelectronics	Performances	Ref.
g-C_3N_4		π-electron system	Fluorescent sensor for trithiocyanuric acid and Hg^+	Trithiocyanuric acid detection limit: (LOD) ~ 9.6×10^{-8} M; Hg^+: range ~ 0–60 μM, LOD ~ 6.2×10^{-7} M	43
		Biocompatibility, controllable band-gap luminescence	Electrochemiluminescence biosensor for DNA methyltransferase	Range ~ 0.05–80 U mL^{-1}, LOD ~ 0.043 U mL^{-1}	44
		Photoactivity	Two-photon steered bone regeneration	Restored area to 91.1% ± 3.2% after 4 weeks	45
		Large surface, photoluminescence	Ratiometric fluorescent probe for H_2O_2 and glucose	H_2O_2: range ~ 0.5–50 μM, LOD ~ 50 nM; glucose: range ~ 4–42 μM, LOD ~ 0.4 μM	46
		Catalytic properties, photoinduced electron transfer	Ratiometric fluorescence detection of exosomal protein	Range ~ 2.5–100 ng mL^{-1}, LOD ~ 2.5×10^3 particles mL^{-1}	47
		Conductivity, biocompatibility	Electrochemical detection of serotonin	Range ~ 500 pM–1000 nM, LOD ~ 150 pM	48
		Biocompatibility, fluorescent	Fluorescence probe for detection of hemin	Range ~ 0.5–25 μM, LOD ~ 0.15 μM	49
BP		Conductivity	FET biosensor for human IgG	Range ~ 2–100 ng mL^{-1}, LOD ~ 10 ng mL^{-1}	50
		Photoresponse	Synapse	Energy consumption ~3.5 pJ	51
		Large surface, conductivity	Electrochemical detection of myoglobin	Range ~ 1 pg mL^{-1}–16 μg mL^{-1}, LOD ~ 0.524 pg mL^{-1}	52
		Large surface, negative electricity	Fluorometric method for protease detection	Range ~ 0–15 ng mL^{-1}, LOD ~ 1 ng mL^{-1}	53
		Light absorbance	Fluorometric method for miRNA detection	Range ~ 1–1000 nM, LOD ~ 0.96 nM	54
TMDs	MoS_2	Large surface, flexibility, semiconducting	Tactile sensor	Pressure range ~ 1–120 kPa, response time ~ 180 ms	55
	MoS_2	Transparency, flexibility, ultrathin, semiconducting	Tactile sensor	Pressure range ~ 1–40 kPa; LOD ~ 1.24 kPa; gauge factor ~72.5	56
	MoS_2	Large surface, conductivity, catalytic properties	Electrochemical detection of roxarsone	Range ~ 0.05–490 μM, LOD ~ 0.03 μM	57
	MoS_2	Electroactivity, differential affinity toward single and double-stranded DNA	Electrochemical detection of DNA hybridization	Range ~ 0.03–300 nM	58
	MoS_2	Large surface, semiconducting	FET for DNA hybridization detection	LOD ~ 10 fM	59
	MoS_2	Semiconducting	FET for prostate-specific antigens detection	LOD ~ 375 fM	60
	MoS_2	Atomically thin, semiconducting	FET for streptavidin detection	sensitivity ~196 at 100 fM	61
	MoS_2	Quantum confinement effect, semiconducting	FET for glucose detection	Range ~ 300 nM–30 mM, LOD ~ 300 nM	62
	MoS_2	Lattice distortion	Memristor	Stable in 1000 sweeping cycles	63
	MoS_2	Conductivity	Synapse	Energy consumption ~4.8 pJ	64
	WSe_2	Large surface, semiconducting	Biosensor for SARS-CoV-2	LOD ~ 25 fg μL^{-1}	65
	WS_2	Large bandgap	Memristor	Switching times ~13 ns	66
MXene	Ti_3C_2	Large surface, conductivity, biocompatibility	FET for dopamine detection	Range ~ 100×10^{-9}–50×10^{-6} M, LOD ~ 100×10^{-9} M, temporal resolution ~50 ms	67

TABLE 1 (Continued)

		Characteristics	Bioelectronics	Performances	Ref.
	Ti_3C_2	Conductivity, large surface, catalytic properties	Chemiluminescence detection for exosomes	LOD ~ 125 particles μL^{-1}, 100 times lower than ELISA method	68
	Ti_3C_2	Conductivity, biocompatibility, dispersibility	Enzyme biosensor for phenol	Range ~ 0.05–15.5 μM, LOD ~ 12 nM	69
	Ti_3C_2	Conductivity, large surface, biocompatibility	Neural interfaces	4-fold reduction in interface impedance than Au electrodes	70
	Ti_3C_2	Flexibility	Pressure sensor	LOD ~ 8 Pa, response ~14 ms, mechanical reversibility ~5000 times	41
	Ti_3C_2	Tunable conductivity, layered structure	Piezoresistive sensor	Mechanical reversibility >4000 times, response <30 ms	72
	$Ti_3C_2X_2$	Semiconducting	Memristor	Energy consumption ~18.82 nJ	72
	$Ti_3C_2X_2$	Electroactivity	Detection of synapse plasticity behavior triggered by neuro-transmitter	Range ~ 1 aM–1 μM, LOD ~ 1 aM	73
MOFs	Zn-TCPP	Large surface	Fluorescence sensor for DNA detection	Range ~ 0–5 × 10^{-9} M, LOD ~ 20 × 10^{-12} M	74
	Zn-TCPP	Large surface	Organic synaptic transistor	On/off ratio > 10,[3] endurance ~500 cycle times	75
	Cu-TCPP	Large surface, π-electron system	Aptasensor for ochratoxin	Range ~ 0.1 fg mL^{-1}–1 μg mL^{-1}, LOD ~ 0.08 fg mL^{-1}	76
	Co-TCPP (Fe)	Large surface	Electrochemical detection of H_2O_2	Range ~ 0.4 × 10^{-6}–50 × 10^{-6} M, LOD ~ 0.15 × 10^{-6} M	77
	Cu-MOF	Large surface, π-electron system	Electrochemical detection of AA, H_2O_2	AA: range ~ 10–2400 μM, LOD ~ 2.94 μM; H_2O_2: range ~ 10–1000 μM, LOD ~ 4.1 μM	78
	521-MOF	Large surface, electroactivity	Electrochemical and surface plasmon resonance for mucin 1 detection	Range ~ 0.001–0.5 ng mL^{-1}, LOD ~ 0.65 pg mL^{-1}	79
	NiCo-MOF	Large surface, π-electron system	Electrochemical detection of glucose	Range ~ 1 μM–8 mM, LOD ~ 0.29 μM	80
	Fe-BTC	Large surface, catalytic properties	Enzyme biosensor for H_2O_2 and glucose	H_2O_2: range ~ 0.04–30 μM, LOD ~ 30 nM; glucose: range ~ 0.04–20 μM, LOD ~ 39 nM	81
	Yb-MOF	Large surface, conductivity	Electrochemiluminescence detection for picric acid and berberine chloride form	Picric acid: range ~ 0.1–1 μM, LOD ~ 81.3 nM; berberine chloride form: range ~ 0.05–1 μM, LOD ~ 36.5 μM	82
	CuTCNQ	Conductivity	Pressure sensor	Range ~ 0–1500 Pa, LOD ~ 0.73 Pa, sensitivity ~6.25 kPa^{-1}	83
	Cu-THPP	Semiconducting, ultrathin	Synapse	Realized the STP and LTP	84
	NH_2-MIL-53(Al)	Water solubility, large surface	Ratiometric fluorescent probe for H_2O_2 and glucose	H_2O_2: range ~ 0.5–50 μM, LOD ~ 26.49 nM; glucose: range ~ 4–42 μM, LOD ~ 0.041 μM	85
	Hf-ETTC-MOL	Large surface, porous structure	Electrochemical detection of carcinoembryonic antigen	Range ~ 1 fg mL^{-1}–1 ng mL^{-1}, LOD ~ 0.63 fg mL^{-1}	86

(Continues)

TABLE 1 (Continued)

		Characteristics	Bioelectronics	Performances	Ref.
	$Cu_xNi_{3-x}(HHTP)_2$	Large surface, semiconducting	Aptasensor for C6 glioma cells and EGFR	C6 glioma cells: range ~ 50–1 × 10^5 cells mL^{-1}, LOD ~ 21 cells mL^{-1}; EGFR: range ~ 1 fg mL^{-1}–1 ng mL^{-1}, LOD ~ 0.72 fg mL^{-1}	87
	Ru-MOF	Large surface	Electrochemiluminescence detection for cardiac troponin I	Range ~ 1 fg mL^{-1}–10 ng mL^{-1}, LOD ~ 0.48 fg mL^{-1}	88
COFs	Py-M-COF	Large surface, high charge carrier mobility	Electrochemical aptasensors for enrofloxacin and AMP	Enrofloxacin: range ~ 0.01 pg mL^{-1}–2 ng mL^{-1}, LOD ~ 6.07 fg mL^{-1}; AMP: range ~ 0.001–1000 pg mL^{-1}, LOD ~ 0.04 fg mL^{-1}	89
	TPA-COF	π-electron system, planar structure	Fluorescence sensor for single strand DNA	Range ~ 0–1 nM, LOD ~ 20 pM	90
	p-COF	π-electron system, hydrogen bonding	Aptasensor for EGFR and MCF-7 cells	EGFR: range ~ 0.05–100 pg mL^{-1}, LOD ~ 5.64 fg mL^{-1}; MCF-7: range ~ 500 × 10^5 cell mL^{-1}, LOD ~ 61 cell mL^{-1}	91
	TpTta	π-electron system, planar structure	Fluorescence sensor for single strand DNA and nucleotides	DNA: range ~ 10–100 nM, LOD ~ 3.7 nM; ATP: range ~ 25–200 μM	92
	COF-5	Long-range order porous structure	Alcohol-sensory synapse	Recognition accuracy ~87.2%	93
Metal oxide	MoO_3	Ultrathin, semiconducting	Synaptic transistor	Energy consumption ~9.6 pJ	94
	MoO_3	Layered structure, surface plasmons	Fiber-optic biosensor for bovine serum albumin	LOD ~ 1 pg mL^{-1}	95
	MnO_2	Planar structure, large surface, conductivity, light absorption	Turn-on fluorescent method for detection of AA	Range ~ 0.5–40 μM, LOD ~ 0.09 μM	96
	MnO_2	Catalytic properties	Ratiometric fluorescent sensor for glutathione	Range ~ 20–2000 nM, LOD ~ 6.7 nM	97
	V_2O_5	Redox activity, wide optical band gap	Fluorescent probe for cysteine	Range ~ 0.1–15 μM, LOD ~ 50 nM	98
	SnO_2	Oxygen vacancy defects, atomically thin	Memristor for neuromorphic computing	92.25% learning accuracy	99
Composites	g-C_3N_4/CuO	Semiconducting, catalytic properties	Electrochemical detection of dopamine	Range ~ 2 × 10^{-9}–7.11 × 10^{-5} M, LOD ~ 1.00 × 10^{-10} M	100
	g-C_3N_4/TiO_2	Biocompatibility, large surface, narrow band gap	Electrochemical detection of glucose	Range ~ 0.05–16 mM, LOD ~ 0.01 mM	101
	$BiVO_4$/2D-C_3N_4	Heterostructure, π-electron system	Aptamer photoelectrochemical sensor for Microcystin-LR	Range ~ 5 × 10^{-7}–10 μg mL^{-1}, LOD ~ 4.191 × 10^{-8} μg mL^{-1}	102
	g-C_3N_4 /MnO_2	Biocompatibility, high quantum yields	Electrochemiluminescence resonance energy transfer-based biosensor for glutathione	Range ~ 0.2–100 μM, LOD ~ 0.05 μM	103
	MoS_2/g-C_3N_4	Large surface, biodegradability	Electrochemiluminescent immunosensor for alpha-fetoprotein	Range ~ 0.001–50 ng mL^{-1}, LOD ~ 0.33 pg mL^{-1}	104
	Ce-MOF@g-C_3N_4/Au	Large surface, porous structure	Electrochemiluminescence immunosensor for *N*-terminal pro-B-type natriuretic peptide	Range ~ 0.005–20 ng mL^{-1}, LOD ~ 3.59 pg mL^{-1}	105
	BP/Au	Biodegrability, catalytic properties	Degradable biosensor for carcinoembryonic antigen	Range ~ 1 pg mL^{-1}–10 μg mL^{-1}, LOD ~ 0.98 ng mL^{-1}	106

TABLE 1 (Continued)

	Characteristics	Bioelectronics	Performances	Ref.
PO_x/BP	Flexibility, ultrathin, heterostructure	Memristor for neuromorphic computing	91.4% learning accuracy, on/off ratio ~2×10^7, retention time >10^4 s	107
BP/ReS_2	Heterostructure	Synapse	91.3% learning accuracy	108
MoS_2/Ni	Large surface, catalytic properties, conductivity	Electrochemical detection of glucose	Range to 4 mM, LOD ~ 0.31 μM	109
MoS_2/Au	Large surface, semiconducting	Biosensor for Down syndrome screening	LOD ~ 100 aM	110
MoS_2/ZnO	Heterostructure	Synaptic transistor	On/off ratio ~ 10^4	111
WSe_2/WO_3	Heterostructure	Multigate memristive synapse	Energy consumption ~2.7 pJ	112
WO_{3-x}/WSe	Atomically thin, heterostructure	Synaptic barristor	On/off ratio ~ 10^5, cycling endurance ~10^3 times, retention ~10^3 s	113
Ag/ZrO_2/WS_2/Pt	Rapid ion transport	Memristor for neuromorphic computing	87% learning accuracy	114
WSe_2/$NiPS_3$/$FePSe_3$	Semiconducting	Synaptic transistor	Energy consumption ~30 fJ	115
Cu/MoS_2/Au	Atomically thin, electroactivity	Memristor	Switching voltage ~0.1–0.2 V	116
$Ti_3C_2X_2$/Pt	Conductivity, catalytic properties	Electrochemical detection of H_2O_2	LOD ~ 448 nM	117
$Ti_3C_2X_2$/Au	Conductivity, catalytic properties	Electrochemical detection of glucose	Range ~ 0.1–18 mM, LOD ~ 5.9 μM	118
$Ti_3C_2X_2$/TiO_2	Biocompatibility, large surface, conductivity, catalytic properties	Electrochemical detection of H_2O_2	Range ~ 0.1–380 μM, LOD ~ 14 nM	119
AuNPs/Ni-MOF/CNTs	Flexibility, stretchability, biocompatibility	Electrochemical real-time monitoring of dopamine released	Range ~ 50 nM–15 μM, LOD ~ 10.96 nM, sensitivity ~1250 mA/(cm^2 M)	120
Cu(HBTC)-1/Fe_3O_4-AuNPs	Large surface	Biosensor for H_2O_2 and glucose, aptasensor for sulfadimethoxine	H_2O_2: range ~ 2.86–71.43 nM, LOD ~ 1.1 nM; glucose: range ~ 12.86–257.14 μM, LOD ~ 12.2 nM; sulfadimethoxine: range ~ 0.01–1.15 μM, LOD ~ 0.005 μM	121
Au@Cu_2O-MIL-53(Fe)	Large surface, porous structure	Real-time monitoring of H_2O_2 released from living cells	H_2O_2 released by a single cell ~0.042 fM	122
Au NPs/Yb-TCPP	Heterostructure	Photoelectrochemical aptasensor for SARS-CoV-2	Range ~ 0.5–8 μg mL^{-1}, LOD ~ 72 ng mL^{-1}	123

Abbreviations: 2D, two-dimensional; AA, ascorbic acid; AMP, ampicillin; ascorbic acid; ATP, adenosine triphosphate; BP, black phosphorus; CNT, carbon nanotube; COFs, covalent-organic frameworks; EGFR, epidermal growth factor; ELISA, enzyme-linked immunosorbent assay; FET, field effect transistor; lgG, immunoglobulin G; LOD, limit of detection; LTP, long-term plasticity; MCF-7, Michigan Cancer Foundation-7; MOF, metal–organic frameworks; SARS-CoV-2, Severe Acute Respiratory Syndrome Coronavirus 2; STP, short-term plasticity; TCPP, meso-Tetra(4-carboxyphenyl)porphine; TMD, transition metal dichalcogenide; TPA, imine-linked; TpTta, COF prepared from 1,3,5-triformylphloroglucinol (Tp) and 4,4′,4″-(1,3,5-triazine-2,4,6-triyl)trianiline (Tta).

bioelectronics. Owing to their excellent physicochemical properties, emerging 2D materials and their composites can achieve remarkable flexibility, tunable electrical conductivity, versatile functionalities, and high biocompatibility, thus making them ideal candidates for engineering bioelectronic devices. Table 1 summarizes the characteristics, applications, and performances of the emerging 2D material-based bioelectronic devices.

2.1 | 2D graphitic nitride

Similar to graphite, g-C_3N_4 is a pack of atoms via C-N bonds and weak van der Waals forces linking the adjacent layers and can be obtained by exfoliating from melamine, as shown in Figure 1A.[45] In fact, g-C_3N_4 can be exfoliated directly in an aqueous solution without the addition of surfactants or oxidation treatments.[127]

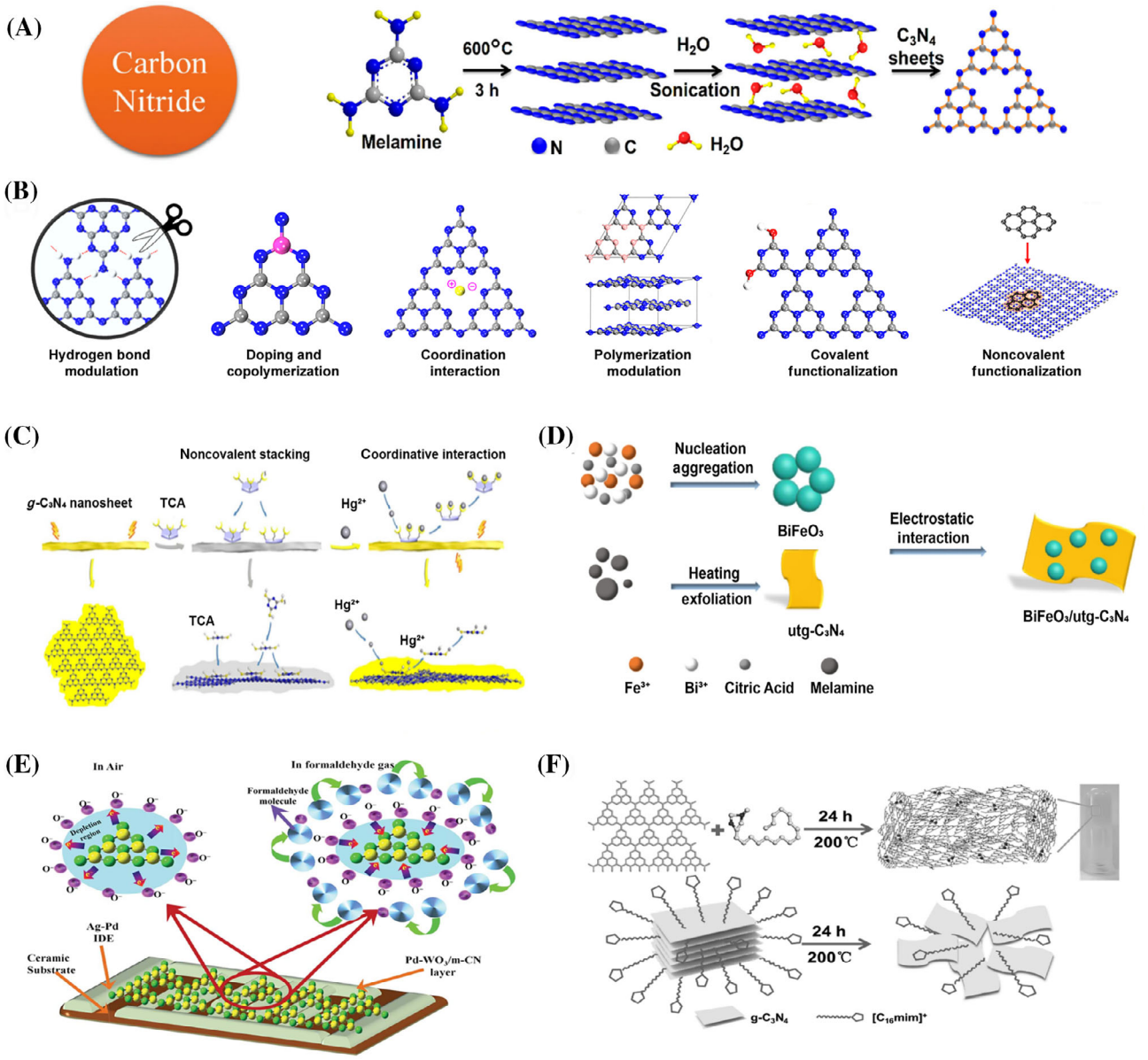

FIGURE 1 (A) Synthesis and characterization of C_3N_4 sheets. Reproduced with permission.[45] Copyright 2017, American Chemical Society. (B) General approaches for engineering the molecular structure of C_3N_4. (C) Mechanism illustration of g-C_3N_4 nanosheets for the detection of TCA and Hg^{2+}. Reproduced with permission.[43] Copyright 2019, Elsevier B.V. (D) Schematic diagram of $BiFeO_3$/utg-C_3N_4 heterojunction. Reproduced with permission.[124] Copyright 2019, Elsevier B.V. (E) Mechanism illustration of Pd-WO_3/m-CN biosensor. Reproduced with permission.[125] Copyright 2018, The Royal Society of Chemistry. (F) Schematic description of g-C_3N_4 hydrogel by hydrothermal method. Reproduced with permission.[126] Copyright 2017, Wiley-VCH. TCA, trithiocyanuric acid

Compared with bulk g-C_3N_4, the ultrathin 2D g-C_3N_4 nanosheets present better water solubility, larger surface area, and tunable bandgap. Meanwhile, other studies have suggested that g-C_3N_4 also displays ultralow cytotoxicity and good tissue compatibility,[128] thus implying that the ultrathin 2D g-C_3N_4 can serve as a suitable candidate for bioelectronics and biosensors. Because bulk g-C_3N_4 can be synthesized from a variety of precursors, it is possible to modify the surface of g-C_3N_4 using the desired molecules, elements, and functional groups. Common design strategies for g-C_3N_4 structures include hydrogen bond modulation, polymerization, coordination, doping and copolymerization, and covalent/non-covalent modifications (Figure 1B).[129] It is well known that covalent chemical modification is an effective way of regulation, including oxidation/carboxylation, polymer grafting, and amidation, which can significantly improve the optical, electronic, and chemical stability of g-C_3N_4.[130] For example,

multifunctionalized g-C_3N_4 prepared by simultaneous chemical binding of amino-coated Fe_3O_4 nanoparticles and CA125 antibody (anti-CA125) on the surface of carboxylated g-C_3N_4 can be used to detect the tumor marker carbohydrate CA125.[131] In addition, noncovalent functionalization, such as π–π stacking, electrostatic interactions, and hydrogen bonding, can also enhance the biocompatibility, reactivity, binding ability, and sensing performance of g-C_3N_4. For example, a fluorescent sensor was developed for detecting trithiocyanuric acid (TCA) and Hg^{2+} by utilizing hydrogen bonds and π–π interactions between TCA and g-C_3N_4, which quenched the fluorescence of the g-C_3N_4 nanosheet solution free of Hg^{2+} when TCA was added. Interestingly, when Hg^{2+} was added again, the S-coordination of Hg^{2+} with TCA destroyed the stacking interaction of TCA-g-C_3N_4, thus restoring the fluorescence (Figure 1C).[43]

In addition to the regulation by covalent/noncovalent means, another commonly used method is the doping of g-C_3N_4. By incorporating external components into the g-C_3N_4 structures, the electrical, optical, luminescent, and magnetic properties of g-C_3N_4 can be regulated. Common doping elements such as O, I, P, Ag, Au, Mn, and SnO_2 have been widely used. For instance, a p-n heterojunction ($BiFeO_3$/utg-C_3N_4) was obtained by electrostatic adsorption based on p-type $BiFeO_3$ nanoparticle-coupled n-type ultrathin graphite-like C_3N_4 (utg-C_3N_4) nanosheets. Owing to the introduction of utg-C_3N_4, the construction of a p-n heterojunction reduced the energy gap of the material and increased the charge separation rate, and was successfully applied to a switched PEC sensor for ampicillin (AMP) determination (Figure 1D).[124] Similarly, a kind of Pd-WO_3/m-CN hybrid nanomaterial, which uses m-CN and WO_3 to form heterojunctions and new electronic barriers with the help of the work function difference between the two materials, has been proven to enhance the sensing ability of Pd-WO_3/m-CN to volatile gases (Figure 1E).[125]

Apart from the introduction of inorganic hybrid materials, g-C_3N_4 can also be composited with new 2D organic structures to construct biosensors to detect protein kinase A (PKA). The sensor used a gold nanoparticle-modified imidazoline nanoskeleton (Au-ZIF-8) as the matrix, carbon microsphere (CMS)-modified ITO as the electrode, and TiO_2-g-C_3N_4 nanocomposite as the photoactive material. The substrate peptide was assembled by the Au-S bond, which was successfully used for the photoelectrochemical (PEC) detection of PKA using the function of substrate immobilization and signal amplification.[132] Moreover, the introduction of MOF during the synthesis of g-C_3N_4, which can improve the dispersibility of the composite and be used as a nerve detoxification medium; a colorimetric detector has also been reported.[133] In addition to the proper structural design of C_3N_4, the selection of appropriate preparation methods can also improve its application. Similarly, a hydrogel-C_3N_4 structure, which was hydrothermally treated at 200°C in the presence of amphiphilic ionic liquids (ILs), was successfully constructed. During this process, carbonitride was peeled off by ILs and gelated to form a hydrogel network, which was deposited layer by layer on the electrode to form a thin film to obtain a chemical resistance sensor and can be used for the detection of hydrogen sulfide (Figure 1F).[126] Although important advances have been made in using C_3N_4-based materials in sensors, significant challenges remain to be overcome. Controllable, large-scale fabrication of high-quality, defect-free ultrathin C_3N_4 nanosheets remains challenging. In addition, the electronic structure and lattice structure of C_3N_4/semiconductor composites need to be studied in detail to fully elucidate the mechanism of C_3N_4-based sensors. In summary, further optimization of the g-C_3N_4 structure can effectively expand its application breadth and depth in the field of bioelectronic devices.

2.2 | 2D black phosphorus

BP has received enormous attention for its atomically thin 2D structures with even higher carrier mobility and structural performance than graphene since 2014.[134–137] The BP nanosheet is an allotrope of phosphorus that can be viewed as a single layer of phosphorus atoms arranged in a hexagon manner, as shown in Figure 2A.[12,145] Every atom in BP is connected to three neighboring atoms forming sp^3 hybridization with a bandgap of approximately 1.5–2 eV for the monolayer BP, thus presenting broad application potentials in electronic devices and biosensors.[146,147] In the 1960s, bulk BP was synthesized, but until 2014, the exfoliation of monolayer BP was reported (Figure 2B).[138,148–150] The synthesis of 2D BP is a big challenge because of its viable reactivity with oxygen, and two main approaches have been proposed: the scotch tape method and liquid-assisted exfoliation.[148] Among the numerous synthetic methods, a top-down exfoliation method is usually used to peel off bulk BP crystals to obtain uniform size and large-scale layered BP nanosheets. For instance, bulk BP was sonicated in an anhydrous polar organic liquid, *N*-methyl-2-pyrrolidone (NMP), under an inert atmosphere, and then centrifuged to collect the 2D BP.[151] So far, many strategies have been proposed to fabricate BP and hybrid-based devices for sensing applications.[152–154] Recently, a spatially controllable aluminum doping technology was proposed that enables p-n homojunction diodes to be implemented within a single 2D BP nanosheet for high-performance photovoltaic applications. Figure 2C illustrates the theoretical electronic structure of the doped double-layer phosphine.[139] They found that the introduction of Al can

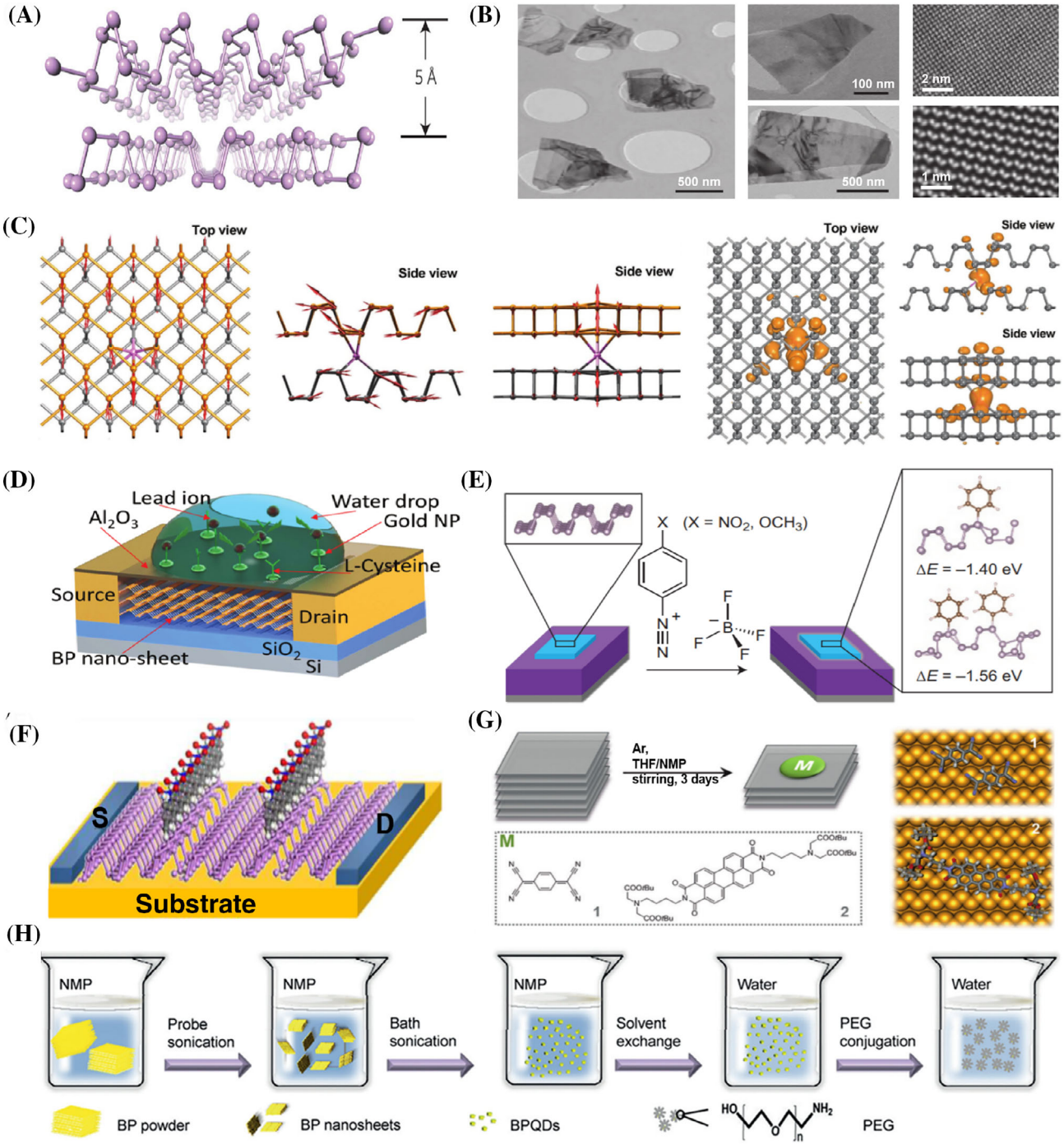

FIGURE 2 (A, B) Atomic structure of BP and SEM/TEM images of BP nanosheets. Reproduced with permission.[12,138] Copyright 2014, 2015, Nature Publishing Group. (C) Theoretical electronic properties of Al-doping in bilayer BP. Reproduced with permission.[139] Copyright 2017, Wiley-VCH. (D) Illustration of ultrathin BP FET transistor. Reproduced with permission.[140] Copyright 2020, The Royal Society of Chemistry. (E) Functionalization of BP by aryl diazo compounds. Reproduced with permission.[141] Copyright 2016, Nature Publishing Group. Schematic representation of (F, G) covalent/noncovalent functionalization of BP. Reproduced with permission.[142,143] Copyright 2016, American Chemical Society. Copyright 2016, Wiley-VCH. (H) Exfoliation of ultrasmall BPQDs and decoration with PEG. Reproduced with permission.[144] Copyright 2015, Wiley-VCH. BP, black phosphorus; BPQDs, BP quantum dots; NMP, *N*-methyl-2-pyrrolidone; PEG, polyethylene glycol; SEM, scanning electron microscopy; TEM, transmission electron microscopy

greatly supply electrons to BP, which can convert the BP fragment from p-type to n-type, significantly improving the electron migration rate of BP, making it a self-powered dynamic photovoltaic and photocurrent electronic device. Moreover, controlling the thickness of BP is an effective method to improve its performance. It was

reported that a location-tracked selective region stripping method for BP could rapidly generate thin BP layers from one to seven layers of atomic thickness, whose good gate control provided a more sensitive response than the traditional BP (Figure 2D). Therefore, the prepared phosphorene-based field effect transistor (FET) (PFET) sensor shows a higher current on/off ratio (300–500) and an excellent lead ion response (1–400 ppb).[140]

BP also offers excellent potential for biomedical applications. Nonetheless, poor chemical stability and uncertain cytotoxicity limit the performance of BP.[155] At present, enhancing the stability of BP mainly includes introducing a surface protective layer, surface chemical modification, and doping of heteroatoms.[156] It has been reported that the stability of BP can be enhanced compared to that of bare BP after being modified with a layer of aluminum oxide (AlO_x) via atomic deposition,[157] without compromising the material properties. In addition, owing to the impermeability of graphene to almost all molecules, the graphene sealing layer has been demonstrated to be able to thoroughly prevent the oxidation of BP. Meanwhile, the graphene layer can be easily removed, which facilitates the operation of BP-based devices.[158] BP can also be modified by covalent/noncovalent functionalization.[142,143] Covalent functionalization alters the properties of BP by forming covalent bonds between BP and other materials, whereas noncovalent functionalization uses surface adsorption. As shown in Figure 2E, the chemical degradation of exfoliated BP is inhibited by coupling lone pair electrons on BP with aryl diazo compounds, such as 4-nitrobenzodiazo, to form P-C covalent bonds.[141] Moreover, polymer modification can not only maintain the transport property of BP, but also improve the stability of polymer-BP composites in ambient conditions (Figure 2F).[142] Noncovalent modification, such as wet chemical treatment of BP with 7,7,8,8-tetracyano hydroquinone (TCNQ) molecule (Figure 2G), can create a reasonably flat energy band in the bandgap of BP, which reduces the hole mobility of BP and significantly improves the antioxidant degradation performance of BP.[143] In addition, surface modification by polymers can also improve the chemical properties of BP, such as biocompatibility (Figure 2H).[144] For example, organosilicon compounds (TMSCl) were used for the surface coordination of BP nanosheets to generate more stable TMSCl@BP, which could maintain its surface morphology and properties for 24 h under ambient conditions and has no cytotoxicity at a concentration of 200 ppm.[159]

The adjustable band gap is the most representative characteristic of layered BP. Moreover, layered BP possesses sufficiently high carrier mobility and a moderate on/off ratio, which makes it particularly appealing in the field of bioelectronics. However, the synthesis and application of layered BP still face many challenges. First, almost all the synthesis methods of layered BP are based on a top-down strategy, which makes it difficult to obtain controllable size and ultra-thin BP. Second, compared with other emerging 2D materials, layered BP is easily degraded in the physiological environment because of its poor chemical stability, which significantly enhances the biocompatibility of BP, for instance, reducing the toxicity caused by its accumulation in vivo to normal tissues and organs, thus offering excellent application potential as biodegradable and implantable electronics or biosensors.[137] However, insufficient stability severely affects electronic performance under ambient conditions. Therefore, improving stability is the key to realizing long-life biological electronics and sensors for layered BP materials.

2.3 | Layered TMDs

TMDs stand out as emerging 2D materials because of their remarkable physicochemical properties and chemical versatility, including large specific surface areas, high mechanical properties, exceptional electronic performance, tunable chemical stability, high catalytic activity, photoluminescence, optical absorption, direct bandgap, and facile synthetic processes, which have received tremendous attention, making them suitable for the construction of ultrasensitive biosensors.[160–163] The promising properties of TMDs will significantly compensate for the deficiency of many other 2D materials, especially graphene-based devices. TMDs are usually characterized as MX_2, where M is a transition metal, for example, Mn, Mo, W, V, and so forth, and X is S, Se, or Te. Bulk TMDs are characterized by covalent in-plane bonding and weak van der Waals interactions between adjacent layers. The crystal structures of the TMDs are shown in Figure 3A.[164] For MoS_2, the monolayer thickness is 6.5 Å. As reported, the layer thickness significantly affected the properties of TMDs.[170] Therefore, controlled synthesis of TMDs is essential for further studies. Two-dimensional TMDs can be exfoliated by physical and chemical means, including tape exfoliation, liquid-assisted exfoliation, and ion intercalation.[171–173] "Bottom-up" synthesis of 2D TMDs has been developed as direct wet chemical synthesis and chemical vapor deposition (CVD) in an attempt to achieve adequate control of layer structure. For CVD, a thin layer of metals or metal compounds is first coated on a substrate and then exposed to a chalcogenide atmosphere to grow the 2D TMDs.

Owing to their direct and tunable bandgaps and excellent physicochemical properties, the state-of-the-art structural design of TMDs is currently the frontier research direction in bioelectronic devices. By carefully controlling the reaction conditions, such as the chalcogen content, emerging 2D materials with unique shapes, such

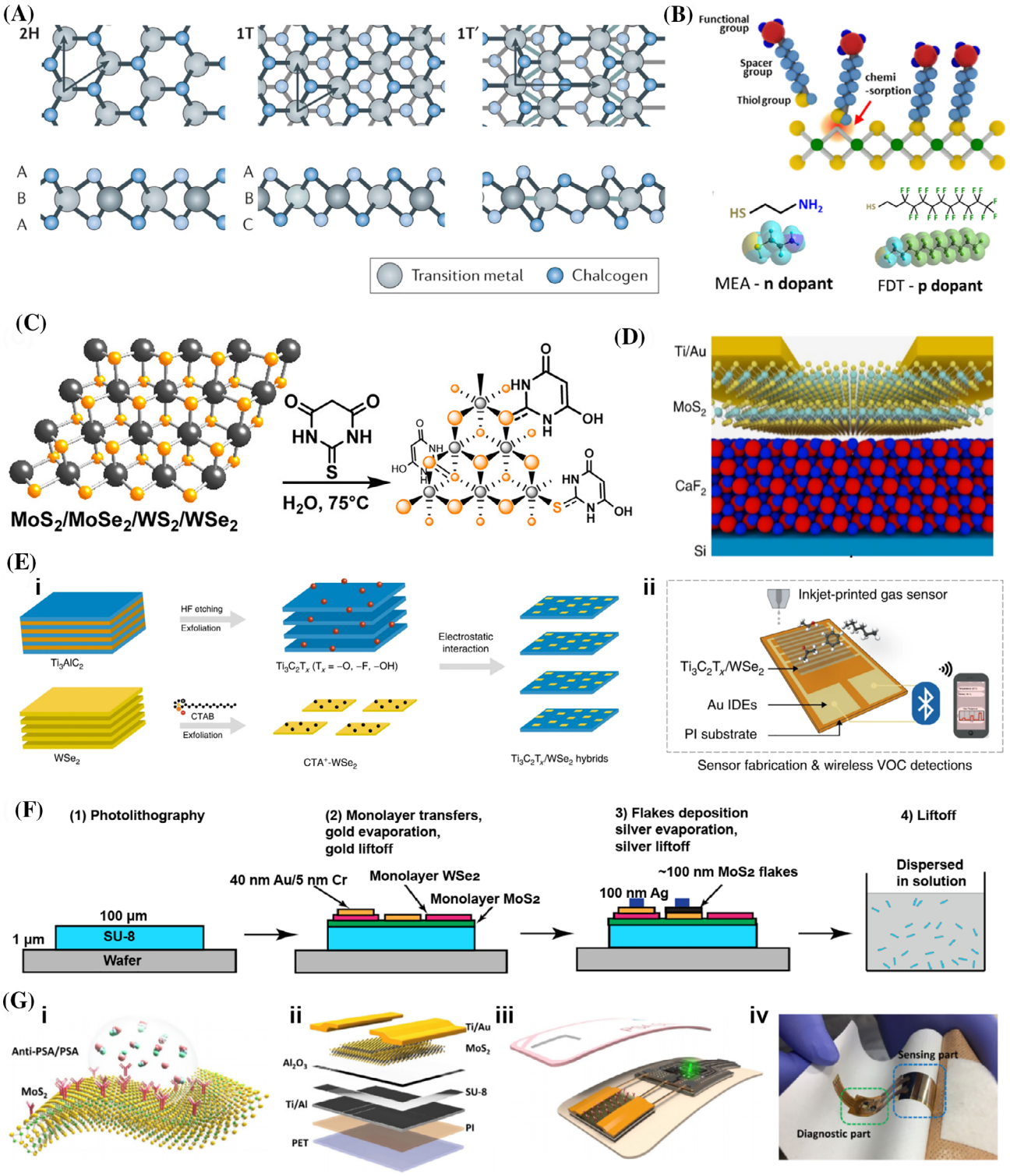

FIGURE 3 (A) Crystal structure of 2D TMDs. Reproduced with permission.[164] Copyright 2017, Nature Publishing Group. (B) Schematic illustration of thiol molecules absorbed on functionalized MoS_2 via thiol chemistry. Reproduced with permission.[165] Copyright 2015, Wiley-VCH. (C) Synthesis of TBA-modified 2D TMDs. Reproduced with permission.[166] Copyright 2017, American Chemical Society. (D) Schematic illustration of F-terminated CaF_2 (111) and MoS_2 hybrid electronics. Reproduced with permission.[167] Copyright 2019, Nature Publishing Group. (E) (i) Synthesis illustration of $Ti_3C_2T_x/WSe_2$ nanohybrids and (ii) inkjet-printed gas sensor system. Reproduced with permission.[168] Copyright 2020, Nature Publishing Group. (F) Fabrication steps of CSM electronics. Reproduced with permission.[169] Copyright 2018, Nature Publishing Group. (G) i–iv Illustration and structure of skin-type MoS_2 biosensor. Reproduced with permission.[36] Copyright 2017, Springer International Publishing AG. 2D, two-dimensional; CSM, colloidal state machine; IDE, interdigital electrode; MEA, mercaptoethylamine; PET, polyethylene terephthalate; PSA, prostate cancer antigen; TBA, thiobarbituric acid; TMD, transition metal dichalcogenide; VOC, volatile organic compound

as triangles, stars, and butterflies, can be obtained.[150] By adjusting the surface defects of low-dimensional materials, such as atomic vacancies and step edges, the structure and function of TMDs can play a crucial role. During the synthesis of MoS_2 or other sulfur-based MS_2 nanostructures, lithium (Li) is inserted between the MoS_2 layers, and because of the violent reactivity of Li, the structure of MoS_2 becomes deformed with high molecular affinity and thiol edge absorption. Hence, thiol molecules can fill up the sulfur vacancies of MoS_2, acting as either donors or acceptors.[31,174–176] In a previous study, mercaptoethylamine (NH_2-terminated thiol, MEA) or 1H,1H,2H,2H-perfluorodecanethiol (CF_3-terminated thiol, FDT) was linked to MoS_2 nanosheets, as shown in Figure 3B.[165] Nowadays, covalent conjugation between lipoic acid and MoS_2 via thiol chemistry has been established as a universal approach for the functionalization of MoS_2 because of its high stability and facile reaction conditions, as shown in Figure 3C.[30,166,177,178] Besides thiol, functionalization by electron transfer between TMDs (MoS_2, WS_2, and $MoSe_2$) and organohalides results in covalent attachment of functional groups to the surface of TMD nanosheets, such as the lone pair electrons in n-type InSe or other 2D materials that can be pulled away from the sulfur atom after being treated by Lewis acids such as $TiCl_4$. The Fermi energy level moves down to the valence band, leading to p-type coordination complexes.[179] Moreover, the performance of TMD-based biosensors can be regulated by hybridization with other 2D materials. For instance, by combining the advantages of $Ti_3C_2T_x$ nanosheets with effective charge transfer and WSe_2 nanosheets with abundant active sites, a $Ti_3C_2T_x/WSe_2$ biosensor for volatile gas sensing could be fine-designed Figure 3E.[168] The hybrid material formed a large number of heterojunction interfaces, which significantly increased the number of adsorbed oxygen species (which in turn trapped more electrons), resulting in a number of electrons released back to the channel, thus improving the detection sensitivity of oxygen-containing volatile organic compounds by more than 12 times.

Currently, owing to the unique semiconducting properties of TMDs, they have shown great potential for technological breakthroughs in sensing applications such as DNA/tactile/gas sensors[56,180–182] and disease detection.[65] As a representative TMD, MoS_2 shows high carrier mobility (60 $cm^2 V^{-1} s$ at 250 K), a layer-dependent bandgap (1.2–1.8 eV), a high transistor on/off ratio (~10^8), and reasonable environmental stability.[183,184] Recent reports have demonstrated that 2D MoS_2 is a desirable channel material in FET sensors with breakthroughs in sensing performance for several fields.[62,65,110,185–188] An ingenious structural design can maximize its abilities. As shown in Figure 3D, a scalable double-layer MoS_2 FET with CaF_2 as the ultrathin gate insulator was fabricated with a thickness of 2 nm and an equivalent oxide thickness of less than 1 nm, compared to conventional silicon-based transistors, to provide better grid control.[167] Similarly, Figure 3F shows a method for the preparation of a functional electronic circuit/transistor/memory and sensor, called a colloidal state machine (CSM),[169] which is fabricated from the top down by h-BN, MoS_2, and WSe_2. By utilizing a combination of a variety of 2D materials, the device not only has the function of memory but also can realize the detection of biosensors, large-area sensors, and sealed space monitors. For disease detection, a MoS_2-based FET biosensor was prepared (Figure 3G).[36] The surface hydrophobicity of MoS_2 can effectively bind anti-prostate cancer antigen (anti-PSA), and this binding process causes direct changes in the electrical properties of MoS_2, such as threshold voltage, field-effect mobility, and subthreshold swing, therefore, it can be used for real-time detection of PSA.

TMDs represent a new class of 2D materials with similar structures and performances to graphene. However, the low electrical conductivity restricts the response rate of TMD-based sensors.[189,190] Researchers have reported various methods to overcome these issues, such as interlayer expansion, phase transformation, composite fabrication with various carbons and conductive polymers, and heterostructure construction with metal compounds.[191,192] For instance, conductive polymers can provide a short diffusion path length for ions/electrons when incorporated with TMDs. In another example, a robust 3D conductive carbon nanotube (CNT)-interpenetrated MoS_2 architecture, in which CNTs penetrate and spread the restacked MoS_2 layers vertically, has been successfully built. This unique structure provides abundant heterointerfaces and enlarged interlayer spacing, facilitating both carrier and phonon transportation in the composites.[193] In addition to these cases, the electrical conductivity may be improved by anchoring conductive nanoparticles or developing metallic TMDs by phase change from the 2H phase to the 1T phase. As TMDs have gradually become one of the most promising emerging 2D materials, the potential risks may raise serious concerns about their practical applications and impact on biological systems. Pumera et al.[194–196] investigated the role of chalcogen atoms in the cytotoxicity of TMDs, which is the chemical reactivity associated with the release of thiogen, thus resulting in higher toxicity. In general, selenium and vanadium play significant roles in toxicity, and the cytotoxicity of ditellurides is higher than that of disulfide-containing materials. Therefore, the atomic composition of TMDs should be carefully considered when designing nanostructures for bioelectronics and biosensors.

2.4 | MXene nanostructures

In recent years, a new type of metal-based 2D material has emerged from the horizon of nanomaterials science,

namely MXenes.[197–202] It is a nanosheet of transition metal carbides and/or carbonitrides produced by removing A layers from $M_{n+1}AX_n$ composites, where M is a transitional metal, A is a group IIIA or IVA, element X is C and/or N, and n is no bigger than 3, the structure of MXenes is shown in Figure 4A.[203] The MAX phases are hexagonally layered with X atoms filling the octahedral sites of closely packed M layers and A atoms interleaving the neighboring layers. Given that the MAX phases can be synthesized with different combinations of M and X, the family of MXenes is quite large, with more than 60 MAX phases being realized.[197] The typical synthesis method was the selective replacement of Al with O, OH, and F from Ti_3AlC_2 using aqueous hydrofluoric acid (HF). In this process, the interlayer interaction is dramatically weakened by the removal of Al, which allows the MX layer to be readily separated into 2D nanosheets.[201,209] Because the n values of $M_{n+1}X_n$ vary from 1 to 3, the 2D MXene consists of three, five, and seven layers of M and X atoms with thicknesses below 1 nm. The properties of MXene can be tuned by the elemental composition and surface terminations, but generally, they show the metallic conductivity of transitional metals and the hydrophilic nature of hydroxyl-terminated nature.[15]

One key factor affecting the properties of MXenes is the interlayer spacing. Generally speaking, MXene obtained by HF etching has a relatively narrow interlayer spacing (±0.98 nm), and its energy storage capacity is limited. To improve this, MXene materials can be utilized because of their high conductivity, large surface area, and tendency to easily accommodate various cations. For example, as shown in Figure 4B, an Na-ion hybrid capacitor with Ti_2CT_x as the anode was well fabricated, in which the interaction/adsorption of Na ions into/onto the surface of MXene enhanced the interlayer distance from 7.7 to 10.1 Å.[204] In addition to cations, conductive polymers can also be used to expand the interlayer spacing of MXenes. For instance, the insertion of polypropylene between Ti_3C_2T layers provided high electrochemical performance and excellent cycle life with a 92% capacitance retention rate after 25 000 cycles (Figure 4C).[74] This is because confining polypropylene to the Ti_3C_2T monolayers leads to high electronic conductivity due to the short diffusion pathway, rapid, reversible oxidation reaction, and better charge transfer. MXenes with tunable hydrophilicity and surface properties are also believed to have promising potential for biomedical applications. Chitosan-linked aerogel sheets of Ti_3C_2X nanosheets exhibit flexibility (can withstand 99% strain), high compressibility (up to 150 000 cycles), and ultrahigh sensitivity, which show great potential in flexible/wearable devices for biological signal detection (Figure 4D).[205]

Moreover, benefiting from a large number of -O or -F on the MXene surface, the performance of MXene can also be improved by adjusting the number of such atoms. For two different concentrations of $Ti_3C_2T_x$ (6 and 15 M), it was found that the capacitance value of $Ti_3C_2T_x$-6 M was much higher because of the presence of more -O functional groups, and more H^+ could enter $Ti_3C_2T_x$-6 M with the increase of H_2O molecules embedded between the interlayers, thereby greatly improving the performance of the electrode (Figure 4E).[206] Another effective method is the preparation of MXene-based composites. For example, as shown in Figure 4F, a multidimensional nanomaterial fabric, which is composed of zero-dimensional nanosilver particles (AgNPs)–one-dimensional silver nanowires (AgNWs)–2D $Ti_3C_2T_x$ nanosheets, has improved the elasticity and conductivity of traditional one-dimensional materials and still ensures the continuity and high sensitivity of materials under considerable strain (200%) owing to the bridge effect of AgNPs.[207] In addition, to regulate the electrochemical performance of MXene, a cetyltrimethylammonium bromide (CTAB) pretreatment was used for the Sn (IV) columnar capacitor CTAB-Sn(IV)@Ti_3C_2 (Figure 4G).[208] The positively charged CTAB can be effectively inserted into the Ti_3C_2 interlayers, thus increasing the interlayer spacing to 2.708 nm, which results in an increase of 177% compared with the original value of 0.977 nm. Moreover, owing to the column effect brought about by Sn(IV), more Li ions can enter the interlayer of MXene, which causes the CTAB-Sn(IV)@Ti_3C_2 anode to have good cycling and rating performance.

Although MXenes have been widely utilized for photocatalysts,[210] electrocatalysts,[211] energy storage,[212,213] electromagnetic interference shielding,[214] and sensors,[215] the etching process greatly affects the condition of MXenes for biomedical applications. For instance, trace amounts of residual HF in biological devices can induce in vivo cell death. In addition, the fluorine-containing etchant induces an abundance of F^- on the surface of MXenes, which is challenging to conjugate via F^- for biomolecules and requires further modification. Therefore, it has been reported that the synthesis of $Ti_3C_2T_x$ MXene can also be achieved through a series of alkaline-induced removal of Al,[216] for instance, the NaOH/KOH-assisted hydrothermal etching process.[217] However, the production of $Ti_3C_2T_x$ under successive NaOH treatment was still very low. The required high temperature (270°C) and NaOH concentration (27.5 mol L^{-1}) would further hamper their scalable production. In addition to alkaline-induced methods, some etching systems involving acidic media or electrochemical etching have also been developed to produce $Ti_3C_2T_x$ MXene, such as electrochemical etching in HCl aqueous electrolyte,[218,219] the modified two-step HCl/KOH

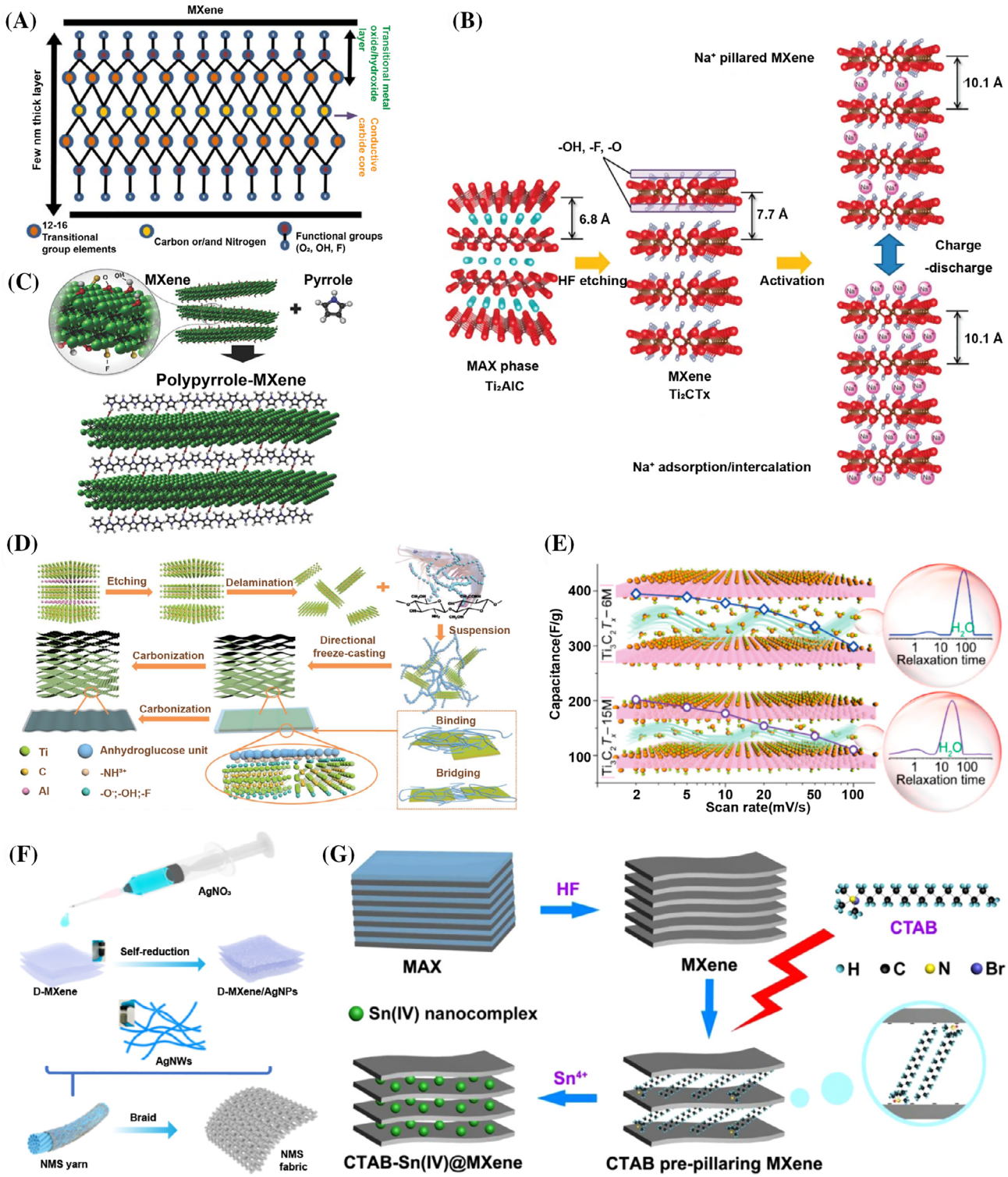

FIGURE 4 (A) Structure of MXene. Reproduced with permission.[203] Copyright 2020, IOP Publishing Ltd. (B) Synthesis of MXene and its reaction mechanism by intercalating and (de)intercalating Na^+ ion. Reproduced with permission.[204] Copyright 2015, Nature Publishing Group. (C) Schematic illustration of pyrrole polymerization using MXene. Reproduced with permission.[74] Copyright 2015, Wiley-VCH. (D) Illustration of fabricating MXene and CS_x/MXene-Caerogels. Reproduced with permission.[205] Copyright 2019, The Royal Society of Chemistry. (E) Capacitive performances of $Ti_3C_2T_x$-6 M and $Ti_3C_2T_x$-15 M electrodes. Reproduced with permission.[206] Copyright 2018, American Chemical Society. (F) Synthesis illustration of NMS fabric, where "N", "M", and "S" stand for nanocomposite, MXene, and silver, respectively. Reproduced with permission.[207] Copyright 2019, The Royal Society of Chemistry. (G) Schematic illustration of the preparation of CTAB-Sn(IV)@Ti_3C_2. Reproduced with permission.[208] Copyright 2017, American Chemical Society. CTAB, cetyltrimethylammonium bromide, HF, hydrofluoric acid

etching method,[220] and electrochemical etching in NH_4Cl/NH_4OH aqueous electrolyte.[221] Moreover, to reduce the waste of the produced acidic/alkaline liquid, a new sustainable molten-salt-assisted electrochemical etching method was developed to synthesize fluorine-free $Ti_3C_2Cl_2$.[222] By adding various inorganic salts, the surface terminations can be modified in situ from -Cl to -O and/or -S, which greatly shortens the modification steps and enriches the types of surface terminations.[223] Thus, exfoliation of MXenes with fluorine-free etchers could control the functional surface termination of MXenes, thus facilitating their use in bioelectronic applications.

Despite the increasing scientific interest in exploring various applications of MXenes, few studies on the toxicity of MXene have been reported. It has been found that the cytotoxicity of MXene may be dependent on the size, preparation process, functional group, oxidative state, dose, and exposure time.[224] As the surface multifunctional strategies for MXenes in the biomedical fields are still in their early stages, the biocompatibility and long-term biosafety of MXene-based bioelectronics remains to be fully explored.[225,226] For instance, the in vivo metabolic pathways of MXenes are still unknown, and long-term internal circulation may accumulate in or even damage normal tissues. In addition, it is necessary to further assess the chemical stability of MXenes, which are less stable in storage and subsequent use, and tend to degrade when exposed to humidity or high temperatures.

2.5 | 2D organic frameworks and polymers

A few years ago, 2D organic frameworks and polymers were realized and explored as a new type of 2D nanoarchitecture for multiple applications. MOFs are compounds consisting of metallic ions, known as secondary building units coordinated to organic ligands (linkers) to form highly porous 3D structures.[227–229] Thousands of MOFs are being discovered every year owing to the variety of metal ions and polymer linkers. Compared with 1D nanofibers and 3D aggregates, the excellent physicochemical properties of 2D nanosheets are due to their short ion transport distance during the ion diffusion and charge-transfer processes.[230] Recently, the exfoliation of 2D MOF nanosheets was reported by ball milling and ultrasonication. By exfoliating the bulk MOF crystals with the assistance of proper solvents such as H_2O, acetone, and methanol, thin-layered MOF nanosheets were obtained.[231,232] Bottom-up syntheses of 2D MOF nanosheets have also been achieved by surfactant-assisted fabrication.[233]

As a new type of 2D nanostructure, the applications of MOFs in bioelectronic sensor devices have been highlighted for their large surface area and high porosity. It has been reported that Cu(II) and Ni(II) ions have been integrated with highly conjugated tricatecholate, that is, 2,3,6,7,10,11-hexaiminotriphenylene (HITP), to form porous 2D MOF nanosheets for gas sensors, as shown in Figure 5A.[241] Similarly, other 2D MOF sensors can detect various species of molecules, such as aromatics, amines, and aliphatic hydrocarbons.[234] The sensor array can also be designed using these 2D MOFs by either drop-coating on the patterned Au electrode surfaces with good sensing capabilities (Figure 5B).[235] In a recent report, such conductive 2D MOFs have been applied to design p-type FET devices, which also have discriminable on/off ratios and excellent field-effect hole mobilities at 48.6 $cm^2\ V^{-1}\ s^{-1}$. However, the lack of electrical conductivity in MOFs has limited their applications in capacitors, batteries, and so forth. Fortunately, the conductivity of MOFs can be further optimized by carefully choosing metal ions/clusters to design institutional building blocks and/or multifunctional objects. For example, as shown in Figure 5C, a Pb-MOF crystal (KGF-1) with a sulfur secondary building unit served as a ligand. By reasonably utilizing the large overlap integrals of Pb-Fe orbitals, KGF-1 takes a robust skeleton with high chemical stability and high conductivity.[236] In addition, in Figure 5D, by modifying the SiO_2 dielectric layer in an organic field-effect transistor (OFET) using the MOF film prepared by liquid phase epitaxy (LPE), and controlling the LPE cycle of SURMOF (HKUST-1, $Cu_3[BTC]_2$, BTC = 1,3,5-benzene tricarboxylate) between 2 and 4 cycles, the MOF films grown on SiO_2/Si substrates are characterized by high crystallinity, homogeneity, and a low dielectric constant, as well as the small interfacial trap density in OFETs; this method can adjust and optimize the charge mobility, threshold voltage, and current switching ratio.[237]

In addition to the MOF structures, researchers have also found that organic molecules can create lightweight porous crystalline COFs with superior charge transport ability.[242] They can be fabricated into both 2D nanosheets and 3D nanoparticles, which mainly depend on the building block structure. In a 2D COF, the bond framework is limited to 2D sheets and stacked into layered columns. To form an ordered COF, the geometric building blocks should be stored in the COF, meaning that rigid building blocks and discrete bond linkages are required for a 2D COF. The studied building blocks for 2D COF include benzenes, biphenyls, anthracenes, triphenylenes, and porphyrins, which are mostly flat aromatic systems. By selecting the building blocks, COFs with different morphologies and pore sizes were obtained.[243] 2D COF nanosheets have also been applied for molecule sensing

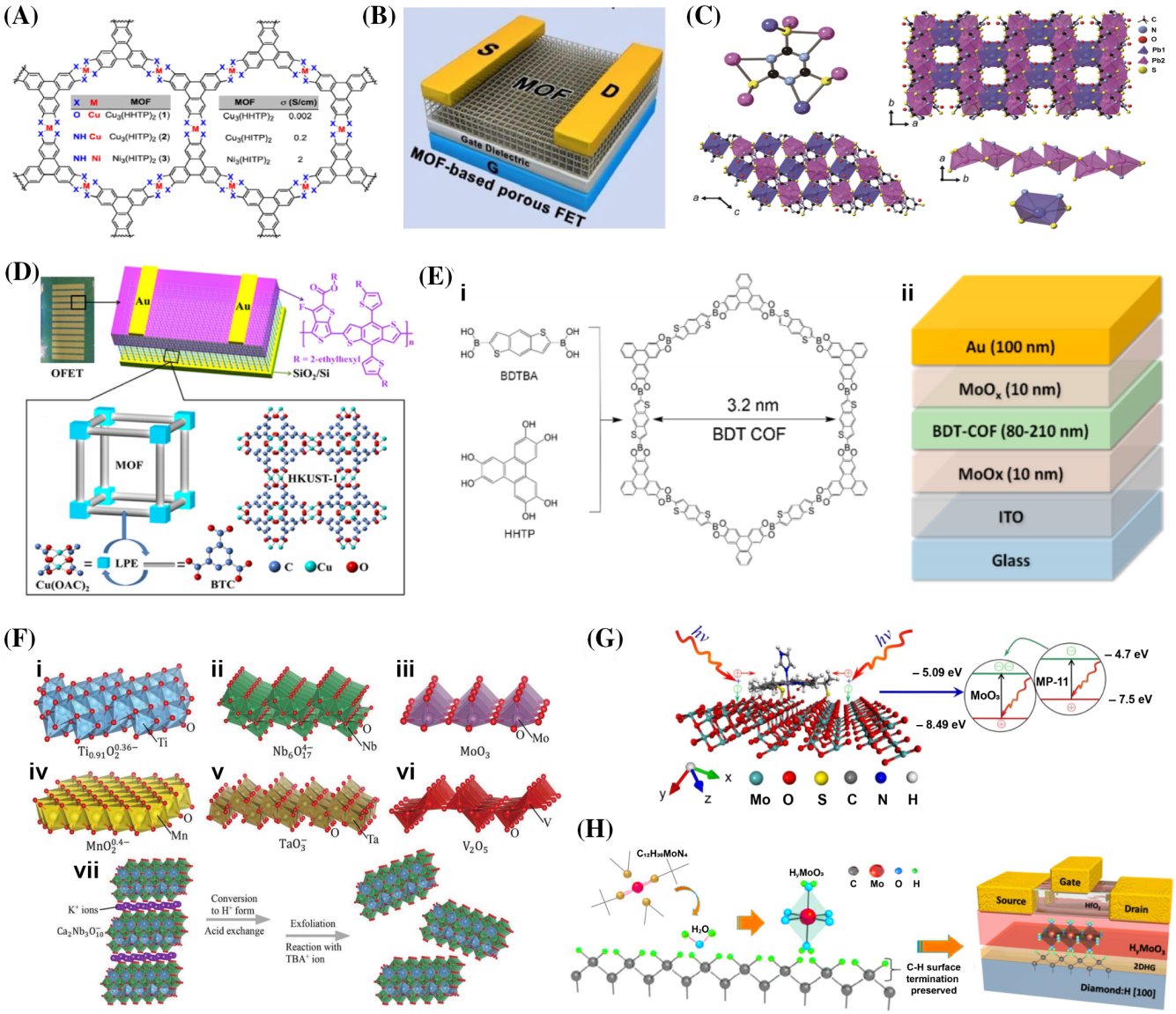

FIGURE 5 (A) The chemical structures of the conductive 2D MOFs ($Cu/Ni_3[HHTP/HITP]_2$). Reproduced with permission.[234] Copyright 2015, American Chemical Society. (B) 2D conductive MOF-based FET devices. Reproduced with permission.[235] Copyright 2017, American Chemical Society. (C) The crystal structure of $Pb_3ttc_2{\cdot}2H_2O$ (KGF-1·H_2O). Reproduced with permission.[236] Copyright 2020, American Chemical Society. (D) Illustration of SURMOF HKUST-1 OFET. Reproduced with permission.[237] Copyright 2017, American Chemical Society. (E) Schematic illustration of BDT-COF; (i) is the schematic representation of BDT-COF; (ii) is the COF hole-only device layout. Reproduced with permission.[238] Copyright 2017, American Chemical Society. (F) Examples of 2D metal oxide nanosheets; (i) is $Ti_{0.91}O_2^{0.36-}$; (ii) is $MnO_2^{0.4-}$; (iii) is Nb_6O^{174-}; (iv) is TaO_3^{-}; (v) is MoO_3; (vi) is V_2O_5. Reproduced with permission.[239] Copyright 2019, Wiley-VCH. (G) Schematic of MP-11 immobilization into the MoO_3. Reproduced with permission.[240] Copyright 2019, Elsevier B.V. (H) Schematic structure of diamond: H/H_yMoO_{3-x} surface and transistor. Reproduced with permission.[258] Copyright 2018, American Association for the Advancement of Science. 2D, two-dimensional; BDT-COF, benzodithiophene covalent-organic frameworks; BTC, 1,3,5-benzene tricarboxylate; FET, field effect transistor; LPE, liquid phase epitaxy; MOFs, metal–organic frameworks; MP-11, microperoxidase-11

or FET devices, which are similar to those of 2D MOF structures.[244–246] Since the first FET 2D COF devices were reported in 2015, 2D COF films have been widely studied as FET devices. For example, highly oriented benzodithiophene COF (BDT-COF) films have both in- and out-of-plane conductivities. Because of the transport barrier between the BDT-COF films, the thickness of the BDT-COF films is related to the measured hole mobility, and the hole mobility of the films is higher than that of thick films (Figure 5E).[238] Recently, a porphyrin-based 2D

COF as an electrochemical aptasensor was prepared for the detection of the antibiotics enrofloxacin and AMP.[89] The high specific surface area and extended π-conjugation throughout the COF skeleton enabled ultrasensitive detection of the antibiotics with an limit of detection (LOD) of 6.07 fg mL^{-1} for enrofloxacin and 0.04 fg mL^{-1} for AMP. Moreover, a 2D MOF-COF nanocomposite (comprising cobalt-based MOF and triazine-based COF) was constructed as an ultrasensitive electrochemical aptasensor for the detection of AMP.[247] It exhibits an extremely low LOD of 0.217 fg mL^{-1} for AMP within a wide detection range varying from 0.001 to 2000 pg mL^{-1}, which is suitable for AMP residue detection in river water, human serum, and milk.

The structural diversity of 2D MOFs and the excellent electrical conductivity of 2D COFs may inspire researchers to explore their potential in the field of biological and biomedical electronics. However, owing to the poor electrical conductivity of 2D MOFs, their practical implementation is restricted. Constructing highly conjugated 2D MOFs or utilizing a combination of conductive substrates such as graphene and CNTs can significantly improve their performance. Considering the application requirements of organic frameworks and polymers for bioelectronics, their properties, such as biocompatibility, biodegradability, and chemical stability, cannot be ignored. Generally, the toxicity properties of MOFs are not only caused by the components of metal ions and organic ligands, but also by the topological structure, biological stability, particle size, and surface compositions.[248,249] COFs usually consist of light atoms, such as C, N, O, and H, which are generally less toxic and more biocompatible than MOFs.[250,251] However, the major limitation of 2D COFs is their poor physiological stability. This is because the reversible nature of the linkages that form 2D COFs increases their biodegradability. Furthermore, owing to the complex molecular arrangements within the 2D organic frameworks and polymers, it is challenging to produce uniform sizes in different batches. Therefore, developing a simple and effective method to achieve scalability, uniformity, and reproducibility during the production process is a great challenge.

2.6 | Metal oxide nanosheets

Apart from the above 2D materials, well-defined 2D metal oxides exhibit better properties than common bulk metal oxides because of their high specific surface areas and highly efficient transport of ions and electrons.[252] In addition, metal oxide nanosheets, such as CuO, ZnO, WO_3, and SnO_2, can be easily synthesized via hydrothermal or solvothermal methods. Figure 5F shows typical 2D metal oxide structures and preparation methods.[239] 2D metal oxides with layered atomic structures show high sensitivity owing to the change in electrical resistance when contacting analyte molecules. Recent studies have provided access to a broad range of atomic 2D metal oxide nanosheets.[253] Currently, diverse types of metal oxides have been intensively studied to serve as sensing materials because of their superficial area, and the potential chemical reactions to small molecules may occur at their interface.[254]

Despite the direct use of metal oxide nanosheets for sensing applications, the integration of heterogeneous metal oxide nanostructures could be another potential pathway for designing and integrating specific sensing capabilities, especially with good sensitivity and selectivity to targeted molecules.[255] For example, 2D metal oxides have been used to fabricate different 3D superstructures, which have gained significant attention for optimizing the surface area and porosity of the electrode.[256] Further surface decoration of diverse semiconducting nanoparticles can further tune their intrinsic sensing capabilities.[239,257] For example, as shown in Figure 5G, the synergistic effect and band arrangement between the two entities in the hybrid material self-assembled from layered MoO_3 and microperoxidase-11 (MP-11) significantly enhanced its biocatalysis and photocurrent conversion.[240] In addition, the surface charge doping of 2D metal oxides has expanded the exploration of 2D metal oxides as FET devices. As shown in Figure 5H, a general strategy has been proposed for using the hydrogenated MoO_3 layer as the electrical structure of the diamond instantaneous surface acceptor layer, that is, the diamond: h/H_yMoO_{3-x} interface.[258] The FET device fabricated by this new method is stable, durable, and maintains a high work function value (5.9 eV), relatively high carrier density (1.9×10^{13} cm^{-2}), and mobility (19.5 cm^2 V^{-1} s^{-1}), and the introduction of hydrogen also adjusts the structure of MoO_3, resulting in intermediate d–d and π–π interstitial states in the interstitial space, making it most conducive to carrier transport from the 2D hole gas channel to the contact point.

Because most of the various 2D materials originate from their parent van der Waals crystals, their atomic structures are identical to their bulk counterparts, except for some lattice constant difference and slight atomic relaxation.[239] In contrast, most metal oxides feature strong interlayer ionic bonds. The lack of strong interlayer interactions in their 2D forms usually introduces dangling bonds, leading to strong surface polarization, which induces prominent structural reconstructions.[259] For instance, when the thickness of ZnO is less than three or four layers, the as-synthesized ZnO exhibits a graphene-like structure rather than a bulk wurtzite structure.[260] When a polar $LaAlO_3$ thin film is deposited on a nonpolar $SrTiO_3$(001) substrate with a TiO_2 terminated surface, an insulator–metal transition is observed when the thickness of the deposited $LaAlO_3$ layers is larger

than four unit cells.[261] These significant differences from bulk materials might make it challenging to determine the atomistic structures of 2D metal oxides, thus hindering their bioelectronic applications. Therefore, in addition to the synthesis of new 2D metal oxides, it is necessary to identify the atomistic structures of 2D metal oxides from both experimental and theoretical perspectives.

Despite many achievements that have been made in bioelectronic and other biomedical applications, the potential cytotoxicity of 2D metal oxides should be fully addressed. In general, bulk metal oxides are considered to have low toxicity, but their 2D counterparts may have different activities in the body. Two-dimensional metal oxides exhibit rapid in vivo clearance and can be quickly excreted from the body's organs without long-term retention, minimizing tissue exposure to nanomaterials and avoiding potential long-term toxicity. In contrast, several in vitro cell viability reports have suggested that there are certain degrees of cytotoxicity of 2D metal oxides. This may originate from the oxygen sub-stoichiometry of the 2D metal oxides induced by the intensive exposure of metal atoms.[262] In summary, the biocompatibility of 2D metal oxides should be evaluated comprehensively, including in vivo histocompatibility, hemocompatibility, acute/chronic toxicity, and metabolic pathways.

3 | ADVANCED BIOELECTRONICS AND BIOSENSORS USING EMERGING 2D MATERIALS

3.1 | Neural interfaces simulation

Neural interfaces are artificial simulation devices that record the electrical activity of the brain and the action potentials generated by individual neurons and understand the cell–cell coupling phenomenon that occurs in neural networks based on neuroelectrophysiology.[263,264] The device used to record brain electrophysiological activity can be placed in the scalp, under the dura mater, or in the cerebral cortex, providing a large number of electrical signals with a spatial and temporal resolution.[265–267] Similarly, designing neural interfaces using 2D materials focuses on the simulation of neuronal functions, including neural computation and synaptic simulation.

3.1.1 | Neuromorphic computing

The neural recording is one of the most challenging research areas for tissue recording. Ideally, a large injected charge density and low impedance are necessary to achieve high sensitivity, thus, the sensor's probe should be as small as possible so that it can communicate with a single neuron to better adapt to the nervous system tissues. Two-dimensional materials might be a solution to address the problems of the lack of highly conductive, mechanically flexible, and robust material.[268–274] For neuromorphic computing, it breaks von Neumann's framework and is highly parallel, fault-tolerant, energy-efficient, and event-driven information processing systems. Traditional simulators are constructed from silicon-based metals, but they are not suitable for large-scale integration. To adapt to the mechanistic performances of neural tissue, 2D materials are usually integrated with flexible substrates instead of rigid conductors.[275,276]

It has been shown that graphene-based sensors can achieve high-resolution neurophysiological activity recording for a rat brain.[267] The electrodes present great potential to mimic live retinal cells with electrochemical methods and can be altered with water-soluble sucrose carrier needles to see the cat visual cortex ulteriorly. The rapid, highly reproducible, and large-scale manufacturing procedure does not require additional welding or connection between electrodes and wires; therefore, it is considered to have potential applications in neural electrodes. In addition to the widespread use of graphene, other emerging 2D materials, such as transition metal sulfides and metal oxides, can also be used in neural computing. As an example, a multiterminal hybrid memory resistor and transistor based on polycrystalline monolayer molybdenum disulfide (MoS_2) can be used for neural computing (Figure 6Ai).[37] This low-resistance state (LRS)-high-resistance state (HRS) memory transistor has gate adjustability of four orders of magnitude, high cycle durability, and long-term stability (Figure 6Aii,iii). More importantly, it also exhibits long-term potentiation and inhibition, and postsynaptic currents (PSCs) exhibit exponential increases/decreases as a consequence of repeatable positive/negative bias pulses, thus successfully mimicking synaptic excitability and inhibition in organs (Figure 6Aiv). Similarly, an $Ag/ZrO_2/WS_2/Pt$ mixed memory resistor,[114] which has a highly stable memory switch and a centralized ON- and OFF-state voltage distribution that can dramatically reduce the randomness of conductive filaments, as well as complete the neuromorphological simulation in the handwritten recognition data set (Figure 6Bi–iii). Multiterminal memory resistor devices are possible candidates for neural computation, but their filament formation mechanism limits their accuracy and energy efficiency. Therefore, an all-solid-state electrochemical transistor was designed, which does not require filament formation and uses lithium ion-based solid dielectric and 2D MoO_3 nanosheets as channels to achieve short-/long-term synaptic plasticity and bidirectional near-linear simulation (Figure 6Ci,ii).[40] Moreover, in the recognition of handwritten digital datasets, the recognition rates of large or small handwritten data reached 94.1% and 87.3%, respectively (Figure 6Ciii,vi).

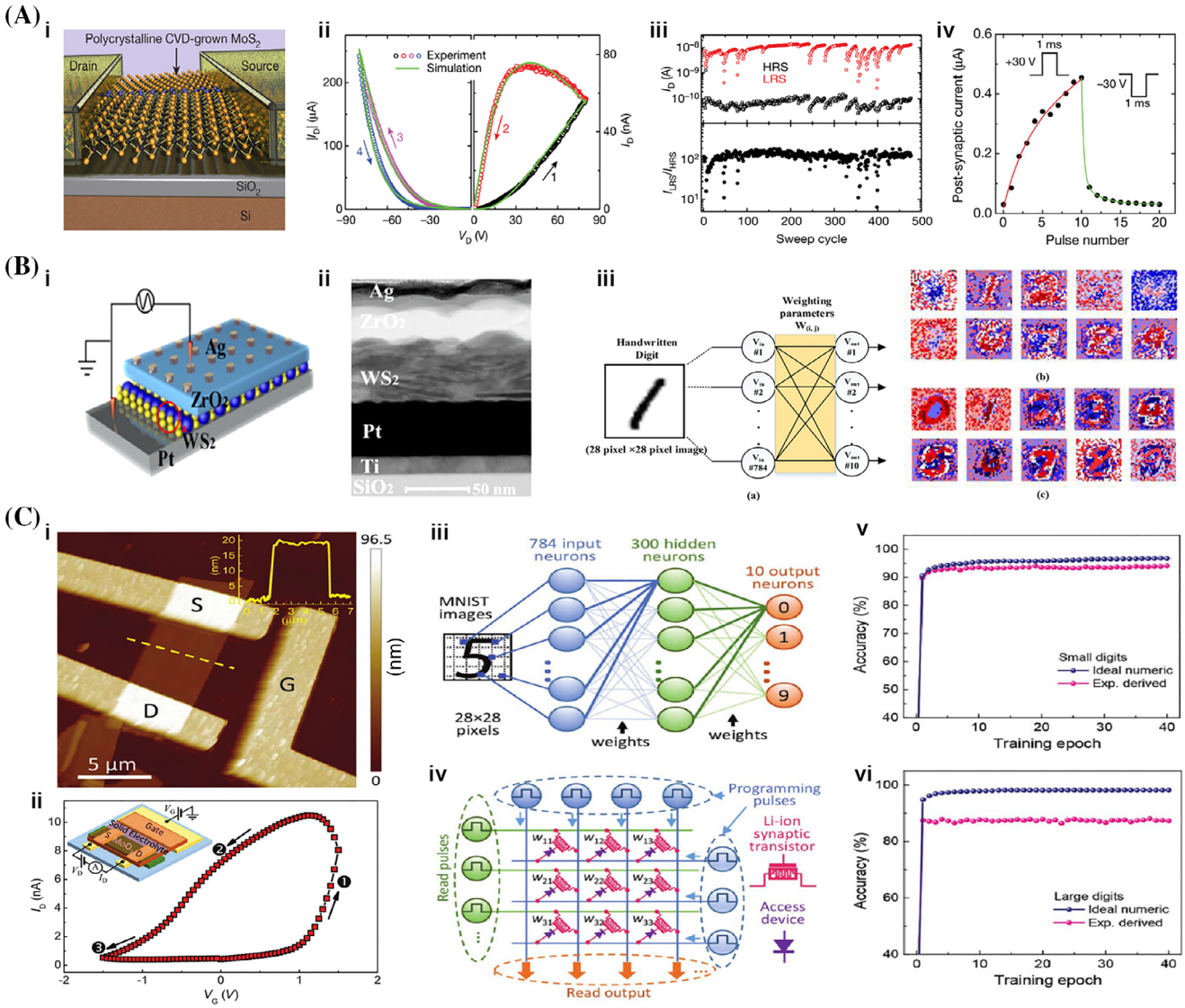

FIGURE 6 (A) (i) Schematic of a MoS_2 memtransistor on SiO_2-Si (gate); (ii) I_D–V_D curve of MoS_2 memtransistor at $V_G = 10$ V; (iii) Endurance of the current and I_{LRS}/I_{HRS} for 475 cycles at $V_D = 0.5$ V; (iv) The long-term potentiation/depression of MoS_2 memtransistor at 30-V and −30-V pulses. Reproduced with permission.[37] Copyright 2018, Nature Publishing Group. (B) (i, ii) Structure illustration and TEM image of Ag/ZrO_2/WS_2/Pt memristor devices; (iii) The working frame of the ANN system and the weighted parameter mapping identification to numbers by memristor devices. Reproduced with permission.[114] Copyright 2019, American Chemical Society. (C) (i) AFM image of the α-MoO_3 transistor; (ii) the schematic illustration and the channel current (I_D) dependence of the transistor; (iii, iv) The schematics three-layer neural network and synaptic weight layer. (v–vi) Handwritten digit image recognition: accuracy-time figures, 8 × 8 pixels, and 28 × 28 pixels, receptively. Reproduced with permission.[40] Copyright 2018, Wiley-VCH. AFM, atomic force microscopy; ANN, artificial neural network; CVD, chemical vapor deposition; HRS, high-resistance state; LRS, low-resistance state; MNIST, Modified national institute of standards and technology; TEM, transmission electron microscopy

3.1.2 | Synaptic transistor

Artificial synapses, as well as neurocomputing that use electronic devices to stimulate the functions of the nervous system, are widely considered the original thought in building a human-like computer or artificial intelligence devices with hardware.[277,278] Current research on artificial synapses has focused on the simulation of biological synaptic capabilities using transistors of different materials, such as floating-gate,[279] electrolyte-gate,[280] ferroelectric-gate,[281] and photosynaptic transistors.[282] Various materials, such as semiconductor CNTs, gold and silver nanoparticles, and polymers, can be used in artificial synapses.[283–285] Similarly, emerging 2D materials have shown promising application prospects in many new electronic applications owing to their unique material properties.[286,287] For example, 2D van der Waals layered crystals and quasi-2D transition metal oxide

semiconductor materials have been used in bioneuron-inspired synaptic transistors.[94]

As another example of a 2D material-based synaptic transistor, Wang et al.[288] first reported a multifunctional synaptic transistor based on a MoS_2/perylene-3,4,9,10-tetracarboxylic dianhydride (PTCDA) hybrid structure using the energy band arrangement between 2D inorganic/organic semiconductors, which achieves robust electro-optic modulation through carrier transfer at the heterojunction interface (Figure 7Ai–ii). By increasing the number of electrons, the minimum inhibition rate and maximum facilitation rate are 3% and 500%, respectively (Figure 7Aiii). The flexible short-term plasticity (STP) and adjustable long-term plasticity (LTP) make this transistor with remarkable STP and LTP and is much superior to other reported transistors (Figure 7Aiv). In addition to changing the band arrangement, constructing ion-gated modulated synaptic transistors is an efficient synaptic simulation device. As an example, a transistor made from layered WSe_2 and phosphorus trihalides can cause different poststimulus diffusion kinetics through surface adsorption and embedding in channel media (Figure 7Ci).[115] It also exhibits excellent STP/LTP transition at different frequencies, excellent repeatability, and linearity, as well as biosynapse-like energy expenditure, resulting in a variety of STP and LTP (Figure 7Cii–v). Moreover, the rapid regulation of synaptic activity can improve the efficiency of artificial synapse simulations. A three-terminal "synaptic barrister", constructing a monolithic tungsten oxide memory resistor and a variable barrier tungsten self-melting point/graphene Schottky diode are shown in Figure 7Bi,ii.[113] Changes in the

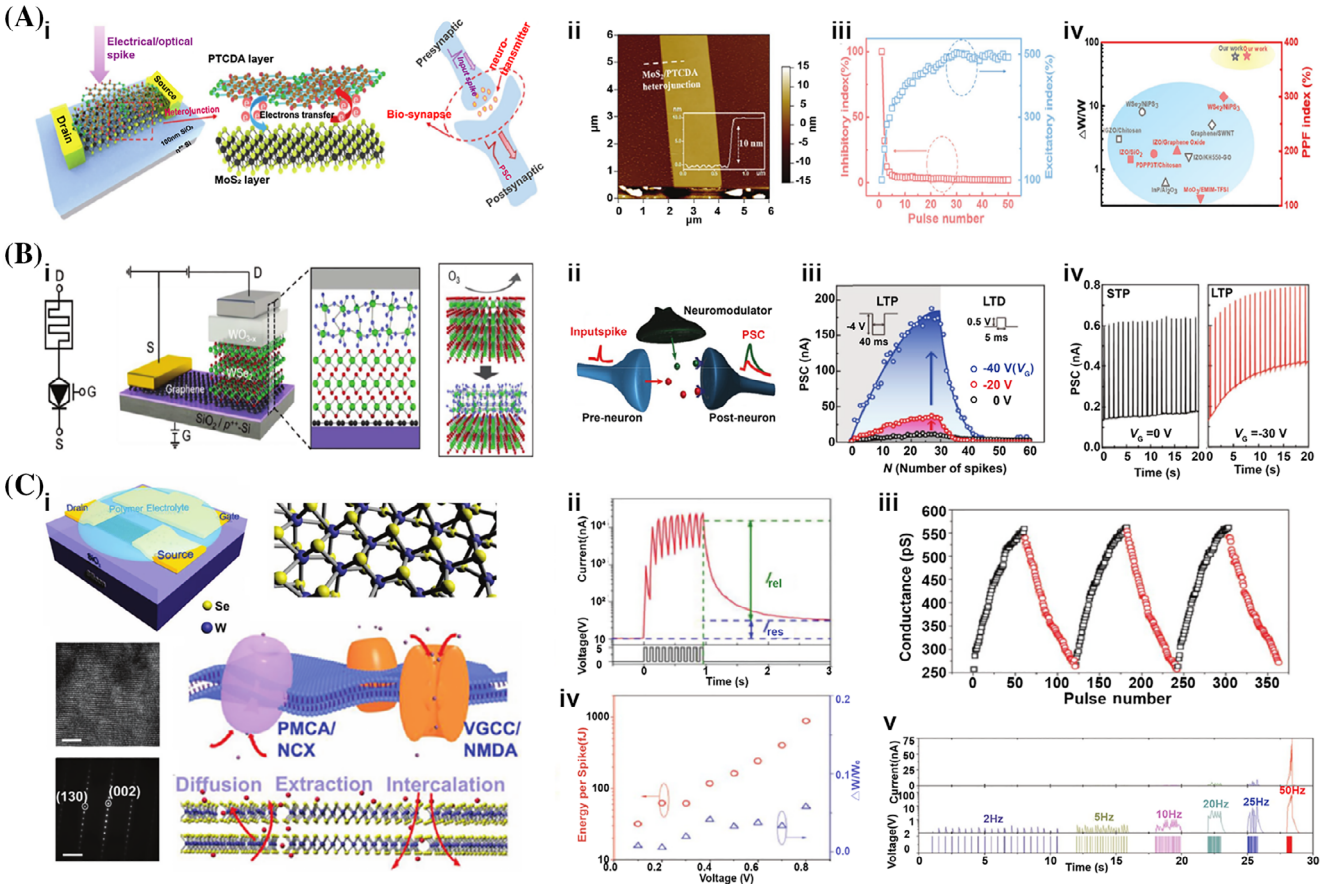

FIGURE 7 (A) (i) Schematic of the MoS_2/PTCDA hybrid synaptic transistor and the biological synaptic diagram; (ii) AFM image of the MoS_2/PTCDA synaptic transistor; (iii) pulse number of the artificial synaptic transistor; (iv) comparison of weight changes and PPF ratios of artificial synapses with those in reported study. Reproduced with permission.[288] Copyright 2019, Wiley-VCH. (B) WO_{3-x}/WSe_2/graphene barrister: (i) the schematic illustration and the monolithic oxidation process; (ii) the corresponding circuit diagram. (iii–iv) Changes of the PSC while applying numbers of spikes as a function of numbers/time at $V_D = -0.1$ V. Reproduced with permission.[113] Copyright 2018, Wiley-VCH. (C) (i) Schematic of the WSe_2 synaptic transistors, HRTEM images, and the similarity of biosynapse, scale bar = 5 nm; (ii) the I_{ds} response as a consequence of STP to LTP transition; (iii) the linearity, symmetry, and reproducibility of the long-term potentiated and depressed WSe_2 synaptic transistor; (iv) function of energy consumption and long-term weight change at 100 μs pulse width; (v) dynamic filtering characteristic of the synaptic transistor at different frequencies. Reproduced with permission.[115] Copyright 2018, Wiley-VCH. AFM, atomic force microscopy; HRTEM, high resolution transmission electron microscopy; LTD, long-term depression; LTP, long-term plasticity; NCX, Na^+/Ca^{2+} exchangers; NMDA, N-methyl-D-aspartic acid; PMCA, plasma membrane Ca^{2+} ATPase; PPF, paired pulse facilitation; PSC, postsynaptic current; PTCDA, perylene-3,4,9,10-tetracarboxylic dianhydride; STP, short-term plasticity; VGCC, voltage gated calcium channel

WSe_2/graphene Schottky diode cause changes in the electrical field strength of WO_{3-x}, thereby leading to changes in PSC, demonstrating its synaptic plasticity (LTP/LTD, STP/LTP, Figure 7Biii,iv). Therefore, it can moderately organize the synaptic degree/rate of the programmed pulses at the source and drain terminals by electrostatic tuning with the gate terminals, which cannot be accomplished by other reported synaptic devices. These properties make it possible to accelerate the consolidation and transformation of synaptic plasticity, as well as STP and LTP and pair pulsing facilitation of synapses.

3.2 | Detection of biomolecules or biomarkers

In recent years, surveillance biosensors and bioelectronics have developed rapidly in adjustable, wearable, and minimally invasive biomedical devices for disease diagnosis and therapy.[289,290] Two-dimensional nanostructures are a top-rated class of materials in this field because they can fill the mechanical differences between rigid/planar devices and flexible/curved interfaces, and they are also a kind of nanomaterial with therapeutic functions.[291,292] Owing to the structural specificity of emerging 2D materials, their available surface area is tremendous, and any chemisorption on their surface may lead to significant changes in the electrical properties of single or several layers of nanosheets, making them very suitable for detecting chem-/biomolecules.[14,22,128,293]

A typical example of the use of emerging 2D materials as biosensors is the detection of various oxides and reactive oxygen species (ROS). By coating g-C_3N_4 on the ITO electrode, a simple PEC sensor using K_4 [Fe (CN)$_6$] as an electron donor solution (Figure 8Ai,ii) was constructed.[294] The PEC sensor can achieve good linear detection of H_2O_2 under different pH conditions; it also

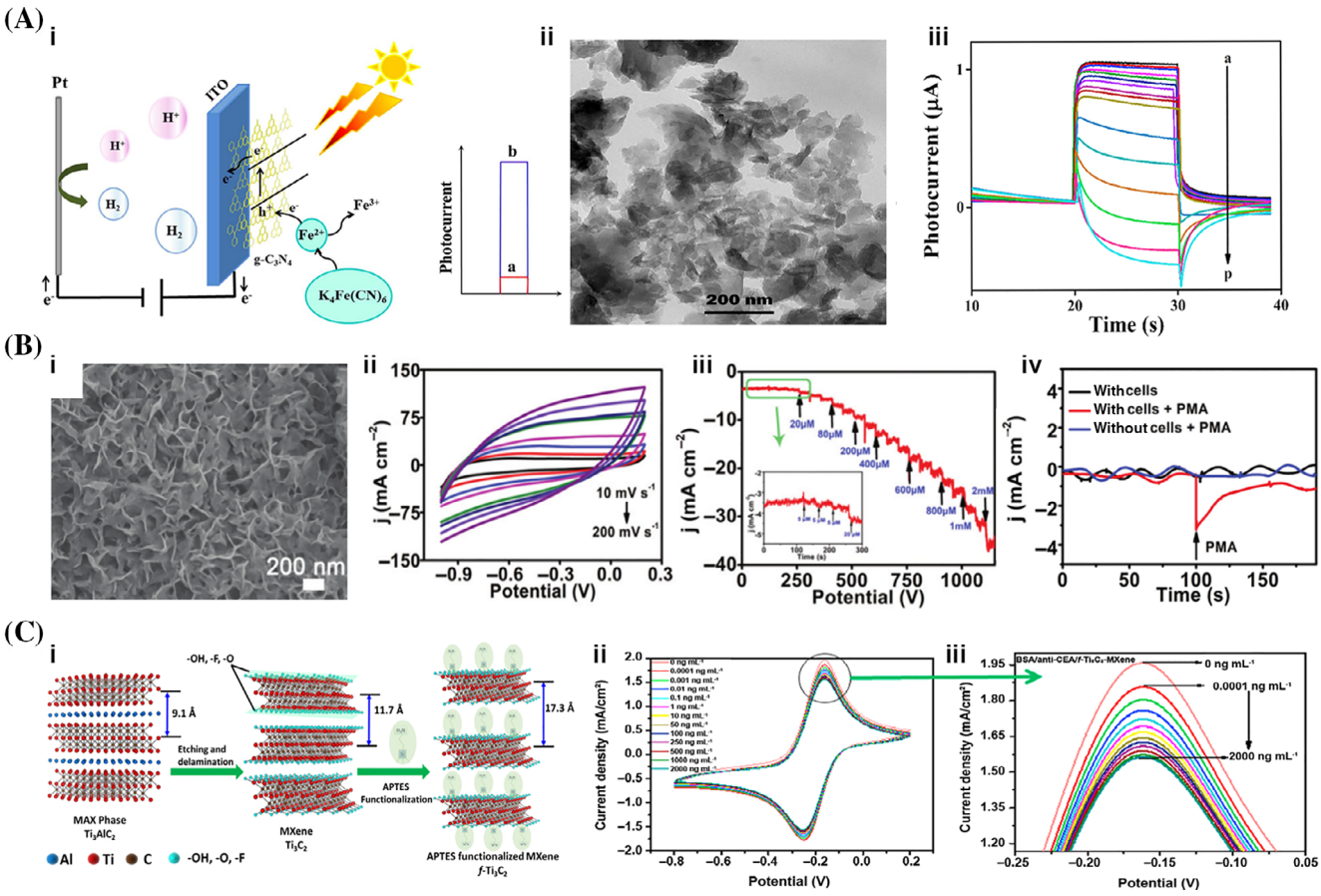

FIGURE 8 (A) (i) Transfer mechanism of g-C_3N_4-K_4[Fe(CN)$_6$]; (ii) TEM image of g-C_3N_4 NSs; (iii) photocurrent response of the g-C_3N_4/ITO electrode in PBS (pH 10) from 0 to 4400 μM. Reproduced with permission.[294] Copyright 2018, Elsevier B.V. (B) (i) SEM images of MoS_2/CC; (ii) cyclic voltammetry of MoS_2/CC in 0.1 M PBS mixed with 1 mM H_2O_2; (iii–iv) the amperometric response of MoS_2/CC in 0.1 M PBS (pH 7.4) (iii) to the continuous addition of H_2O_2 or (iv) with and without A549 cells. Reproduced with permission.[295] Copyright 2019, The Royal Society of Chemistry. (C) (i) Functionalizational diagram of Ti_3C_2-MXene. (ii, iii) Electrochemical sensing performances of BSA/anti-CEA/f-Ti_3C_2-MXene/GC electrode of CEA from 0.0001 to 2000 ng mL^{-1}. Reproduced with permission.[296] Copyright 2018, Elsevier B.V. APTES, aminosilane; CEA, cancer embryonic antigen; ITO, indium–tin oxide; NSs, nanosheets; PBS, phosphate buffer saline; PMA, phorbol-12-myristate-13-acetate; SEM, scanning electron microscopy; TEM, transmission electron microscopy

has a LOD of 0.25–100 μM for ascorbic acid (AA) and 0.5–19 × 10^{-3}% (v/v) for ClO^- at pH 7.4. This sensor has good response characteristics to trace elements and has high specificity, long-term stability, and good reproducibility (Figure 8Aiii). In addition to detecting substances in vitro, emerging 2D materials can detect H_2O_2 in vivo. As shown in Figure 8Bi–iv, a low-cost, self-supporting MoS_2 nanosheet array with good electrocatalytic performance, exhibiting 1.0 μM (S/N = 3) LOD and 5.3 mA mM^{-1} cm^{-2} sensitivity against H_2O_2 in phosphate buffer saline (PBS), and most importantly, it successfully detected trace H_2O_2 secreted by A549 cancer cells in vivo.[295] Emerging 2D materials can also perform ultrasensitive detection of disease markers, such as cancer markers (cancer embryonic antigen [CEA]). Salama et al.[296] synthesized ultrathin Ti_3C_2-MXene nanosheets and functionalized them with amino silane to obtain *f*-Ti_3C_2-MXene (Figure 8Ci). They found that when $[Ru(NH_3)_6]^{3+}$ was used as the redox probe, the detection of anti–CEA-Ti_3C_2-MXene for CEA ranged from 0.0001 to 2000 ng mL^{-1} (Figure 8Cii,iii). The LOD of this *f*-Ti_3C_2-MXene is higher than that of the original 2D nanomaterials and is comparable to that of hybrid emerging 2D materials. Therefore, the use of emerging 2D materials as highly sensitive sensors for DNA, aptamers, enzymes, antibodies, and cells is a new and promising means that can be further applied in the field of in vivo monitoring.

3.3 | Skin sensors and bioelectronics

The emerging 2D materials used in bioelectronic devices have been widely studied. In this section, we provide representative examples of these devices, including skin monitoring, which is one of the most important application fields of 2D materials-based biosensors; it has been found that the 2D materials-based sensor can be constructed and customized based on the application position of skin with tight attachment to the skin without loss of sensitivity for several hours.

The human skin interface is a unique and attractive research field that can be used to monitor temperature, pressure, tactile, and even diseases.[297–299] Therefore, a skin-sensing device (E-skin) composed of 2D materials for detecting various indicators of the human body has been fabricated. In the past 10 years, metal-, graphene-, and conductive polymer-based sensitive E-skins have received tremendous progress.[300,301] However, excessive metal utilization can lead to increased rigidity, high cost, and potential metal ion toxicity. The high electron mobility but near-zero bandgap of graphene might increase the off-state current leakage in graphene-based E-skins, resulting in false signals. Polymers usually possess relatively low conductivities, and their intrinsic conductivity depends on the doped charge carriers. Compared with metal-, graphene-, and polymer-based sensitive E-skins, the emerging 2D materials (e.g., BP[302] and MXene[71]) have many physicochemical advantages, such as a large surface/volume ratio, atomically thinness, mechanical flexibility, high transparency, high carrier transfer characteristics, tunable bandgap and conductivity, and good biocompatibility, which endows them with enormous potential for designing soft and wearable E-skins. Additionally, the quantum confinement effect in atomically thin 2D layers introduces interesting optoelectronic properties and superb photodetection capabilities.[303] Therefore, it is believed that these emerging 2D materials could surpass the performances of these pioneering electronic devices based on metals, graphene, and polymers. Moreover, the emerging 2D materials also show great potential to integrate other unique functionalities when fabricating as E-skin devices, such as photosensitivity, mechanical softness, excellent hydrophilicity, and catalytic properties.

3.3.1 | Physiological monitor

In today's society, everyone is very concerned about personal medical health, which has prompted the flourishing development of medical devices. Among them, portable, intelligent, and wearable medical detection equipment has become an indispensable part of people's daily lives, which is very helpful for diagnosing, treating diseases, and evaluating daily health status. Wearable electronic detection equipment made of 2D materials has the characteristics of high sensitivity, softness, and versatility, and can accurately detect various indicators, including blood glucose concentration, sweat acidity, and alkalinity. Here, a modular, stretchable, and wearable multifunctional sweat biosensor with the solid–liquid-air three-phase interface has been fabricated, which is composed of MXene/Prussian blue ($Ti_3C_2T_x$/PB) composite material as shown in Figure 9A.[39] The product diagram are shown in Figure 9B,C. Owing to the unique 2D morphology and metallic conductivity of $Ti_3C_2T_x$, $Ti_3C_2T_x$/PB composites distinctly improved the electrochemical activity and stability for measuring hydrogen peroxide, and the active sensors in the system are independent and replaceable modules; therefore, different biomarkers can be selected and implanted to detect different indicators. In this report, the sensitivity of the sensor to glucose, lactate, and pH value in artificial sweat and human sweat was tested and proved that it had high electrochemical sensitivity to the concentration of glucose and lactate in artificial sweat as low as 35.3 and 11.4

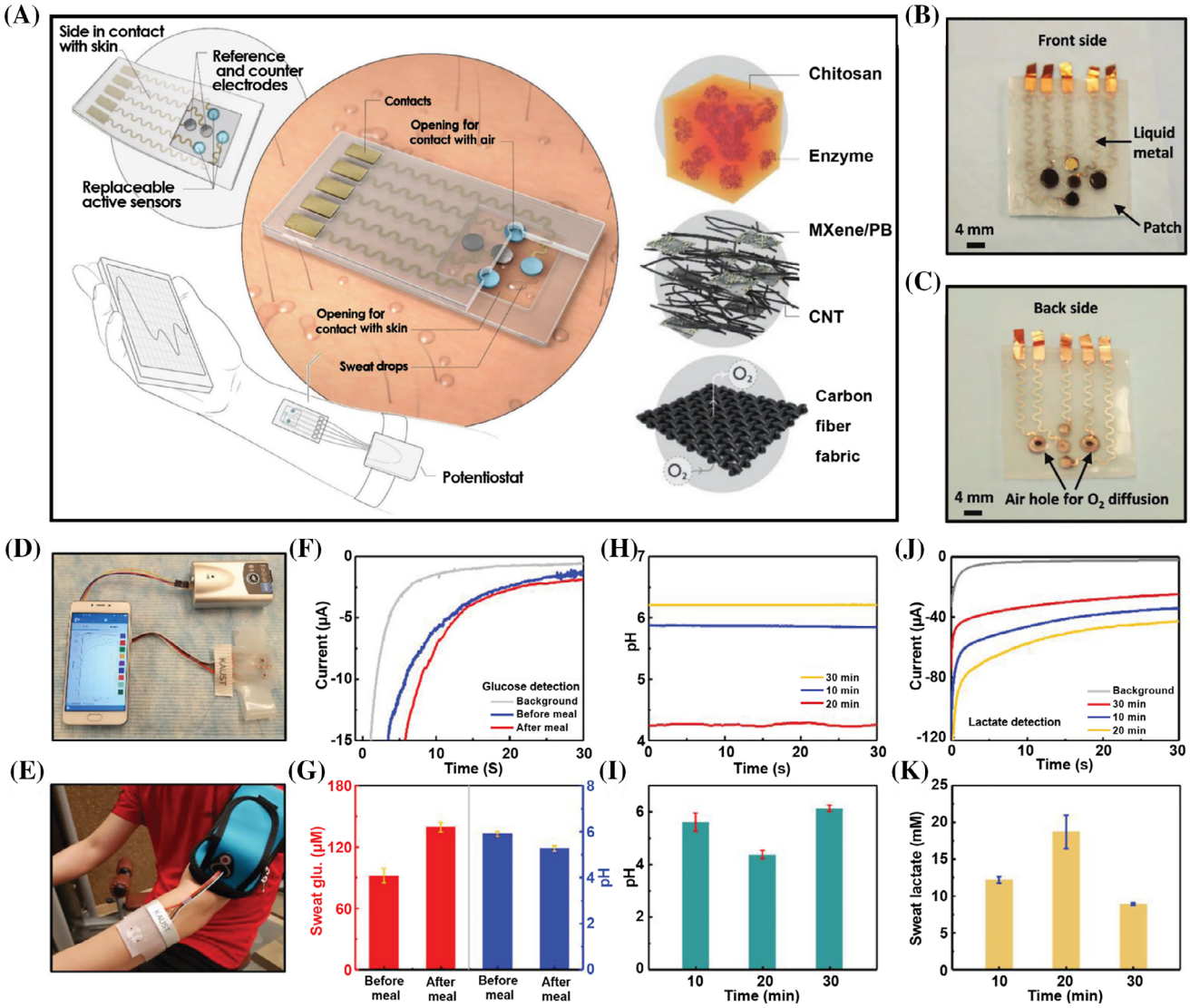

FIGURE 9 (A) Schematic diagram of $Ti_3C_2T_x$/PB sensor and the oxygen-rich enzyme electrode. (B, C) Front/backside optical images of the $Ti_3C_2T_x$/PB sensor. (D, E) Images of real-time evaluation sensing system on the human body. (F–K) The concentrations of pH levels, lactate, and glucose after different treatments. Reproduced with permission from Lei et al.[39] Copyright 2019, Wiley-VCH. CNT, carbon nanotube; PB, Prussian blue

μA mM^{-1} cm^{-2}, respectively. Similarly, it can also measure physiological and chemical signals (glucose/lactate levels and pH changes) simultaneously on human subjects' sweat and maintain high sensitivity and good repeatability, demonstrating its potential for personalized health monitoring (Figure 9D–K). Therefore, this wearable multimode biosensing device can concurrently observe changes in glucose, lactate, and pH values in sweat. This three-phase interface structure is conducive to providing oxygen for the enzyme electrode, thus making the enzyme electrode have a more extensive detection range and ultra-high sensitivity to biomarkers.

In addition to sweat monitoring, emerging 2D materials have been widely used for humidity monitoring. As shown in Figure 10A,B, the WS_2 film can be used as a high humidity sensor under natural flat or high mechanical flexible states and also shows repeatability in the periodically introduced saturated moisture gas sensing Figure 10C.[304] The electronic conductivity of WS_2 endows this device with high sensitivity to the humidity of 90%. When integrated with graphene and thin polydimethylsiloxane (PDMS), a transparent, flexible, and stretchable sensor for humidity monitoring can be fabricated Figure 10D, which can adhere well to the skin and provide a highly stable sensing capability for moisture Figure 10E,F. It has a repeatable humidity response in the stretching, relaxing, and compressing states. When monitoring human breathing in real-time, it is found that it can effectively track relatively fast breathing (1 s) or slower breathing (5 s; Figure 10G,H), thus providing

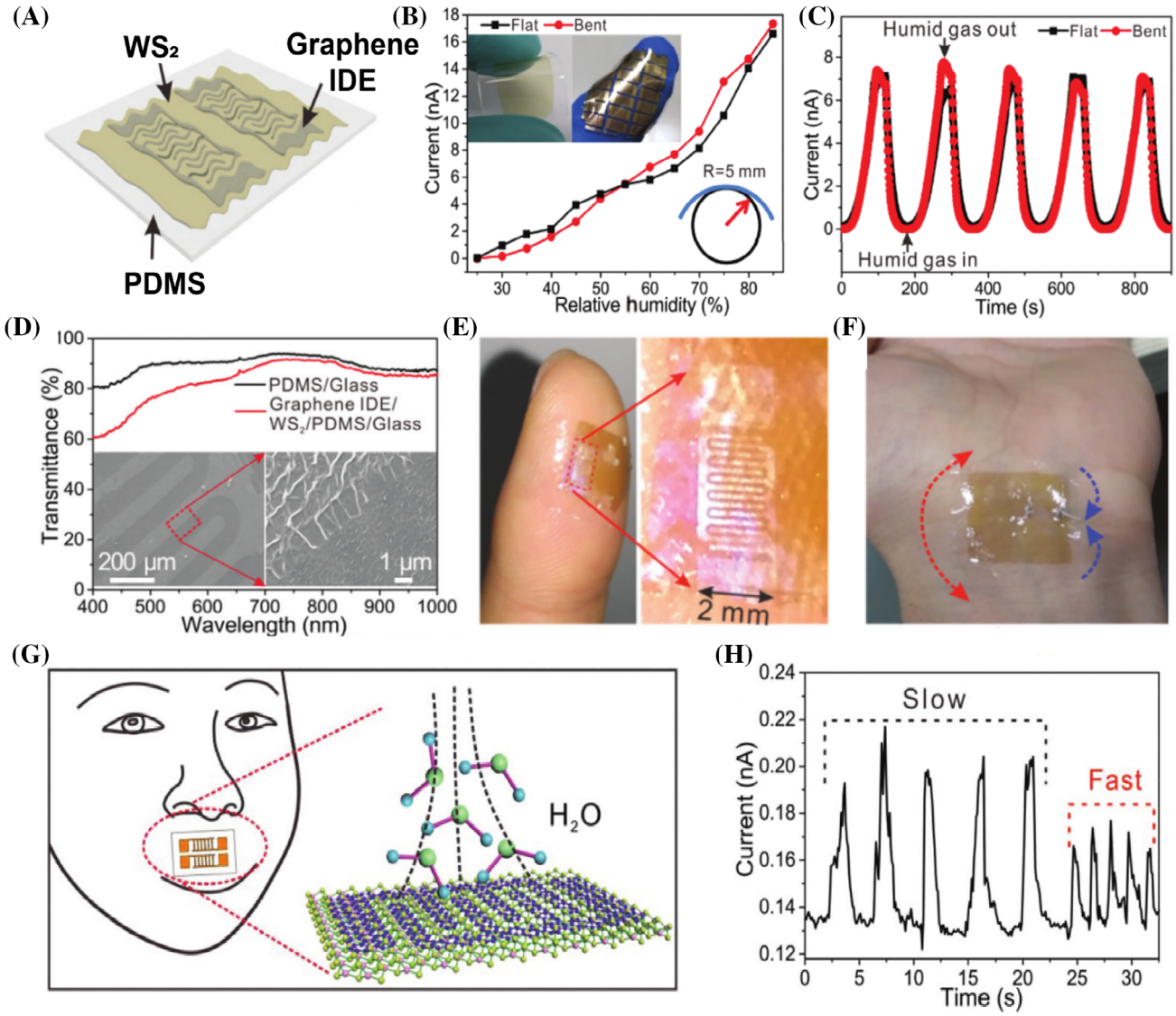

FIGURE 10 (A) Schematic of the WS_2 humidity sensor. (B, C) Humidity performance of WS_2 sensor. (D) Transmittance spectra of WS_2-/graphene/PDMS. (E, F) Photograph of WS_2 sensor attached to a fingertip and waist. (G, H) The sensing performances of the relatively slow and fast respiration rates for the human nose. Reproduced with permission.[304] Copyright 2017, The Royal Society of Chemistry. IDE, interdigital electrode; PDMS, polydimethylsiloxane

great application potential for healthcare monitoring, for instance, the development of low-power consumption wearable chemical sensors.

3.3.2 | Physical-signals monitor

Besides the monitoring of human physiological signals, other physical signals, such as pressure and strain, can also be "visualized" by emerging 2D materials.[305] Pressure sensors based on piezoresistive, capacitive, and triboelectric effects have been achieved based on various types of 2D materials.[306,307] For example, a large-size tactile sensor based on 2D MoS_2 can overcome the interference of crosstalk of traditional passive pressure sensors by placing MoS_2 in the high-k Al_2O_3 layers, thus making the MoS_2 tactile sensor sensing from 1 to 120 kPa, as well as high sensitivity ($\Delta R/R_0$: 0.011 kPa^{-1}) and good linearity response mode (180 ms).[55] The results in Figure 11Ai–iv suggest their excellent application potential for multitouch perception and handwriting recognition.

Based on earlier studies, many CNTs, graphene, and other 2D nanomaterial-based compressible and elastic carbon aerogels (CECAs) exhibit efficient piezoresistive behavior. They can be applied to test tactile contacts with high sensitivity in wearable bioelectronics and E-skins. However, the insufficient interaction between these nanomaterials makes it challenging to fabricate highly

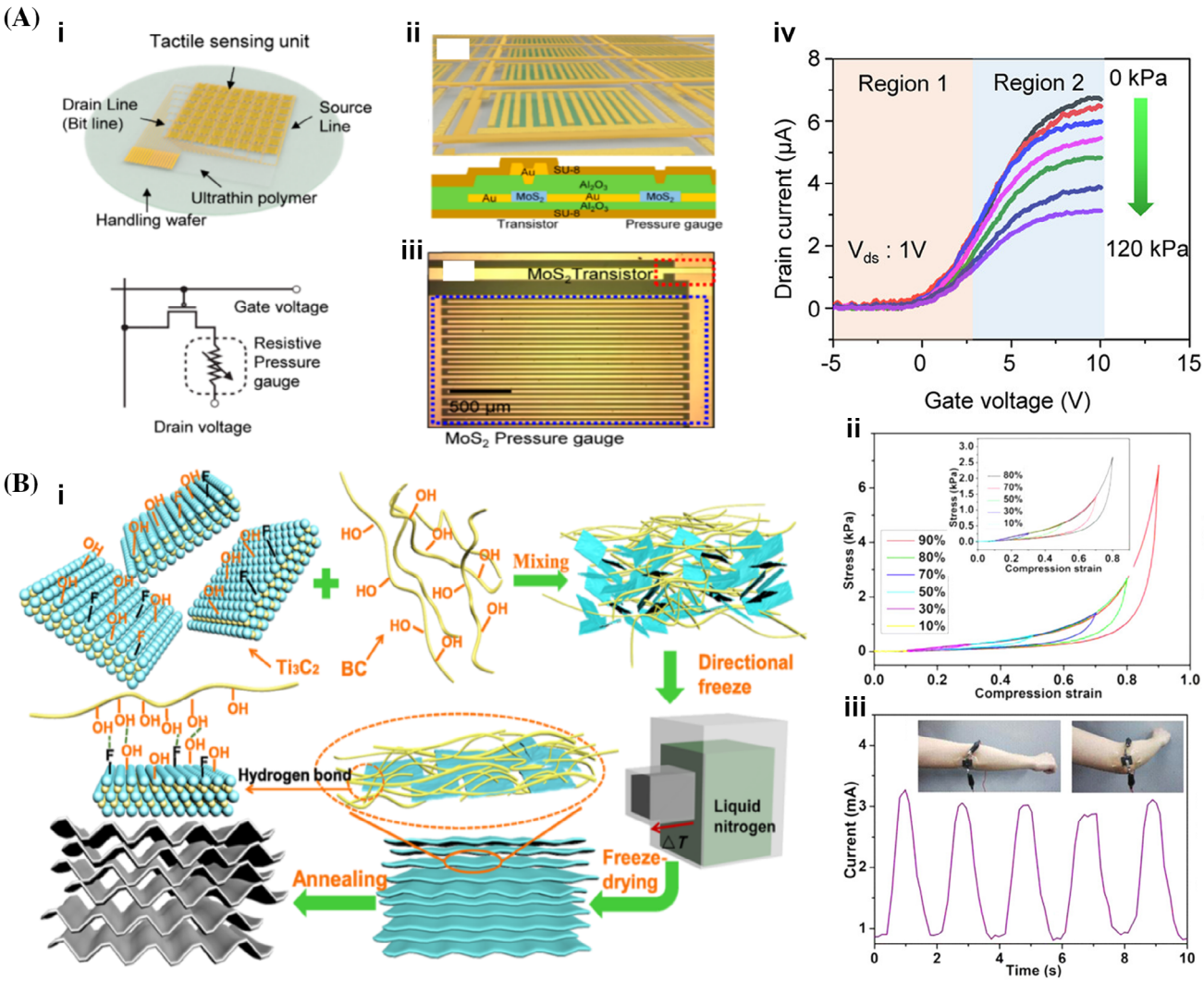

FIGURE 11 (A) (i–iii) The schematic structure and images of the MoS_2 sensor. (iv) Applied pressure-transfer parameters of MoS_2 sensor from 0 to 120 kPa. Reproduced with permission.[55] Copyright 2019, American Chemical Society. (B) (i) Illustration of the fabrication of C-MX/BC-x (C, MX, BC, and x represent carbonization, Ti_3C_2, bacterial cellulose, and the mass ratio of BC to Ti_3C_2, respectively) carbon aerogel. (ii) Stress–strain curves at various compression strains. Current signals from (iii) elbow. Reproduced with permission.[308] Copyright 2019, American Chemical Society. BC, bacterial cellulose

sensitive and robust sensors based on CECAs; therefore, as shown in Figure 11Bi, the bacterial cellulose (BC) as a nanobinder was used to join Ti_3C_2 nanosheets to fabricate a lightweight CECAs for electronic devices.[308] The prepared CECAs showed continuous and wave-shaped/oriented lamellae, resulting in good compressibility (as high as 99% strain for more than 10 000 cycles) and elasticity. As shown in Figure 11Bii,iii, the results show that this device has high sensitivity with a broad working pressure range from 0 to 10 kPa and ultrahigh linearity up to 95% workable strain. Furthermore, it is found that this sensor is very sensitive to subtle strain and pressure changes. When the sensor is attached to the human throat, it can record the current changes from speaking different words, such as "carbon" and "super". Scientists believe that this CECA-based sensor has superior mechanical properties, ultra-high/wide linear sensitivity, and low LOD, indicating a significantly improved possibility of future application of fabricated sensors in wearable sensing devices.

The primary sensing range of most 2D pressure sensors revolves around electronic skin, health monitoring devices, and human–machine interface applications, but are still limited by their specific sensing range, sensitivity, and spatial resolution. An active matrix array based on MoS_2 transistors was reported to monitor various mechanical or biological movements in real-time and can be used in a wide detectable range from footprint to cell movement (Figure 12A–D).[309] The resulting active matrix arrays of mechano-luminescent, air-mediated field-effect

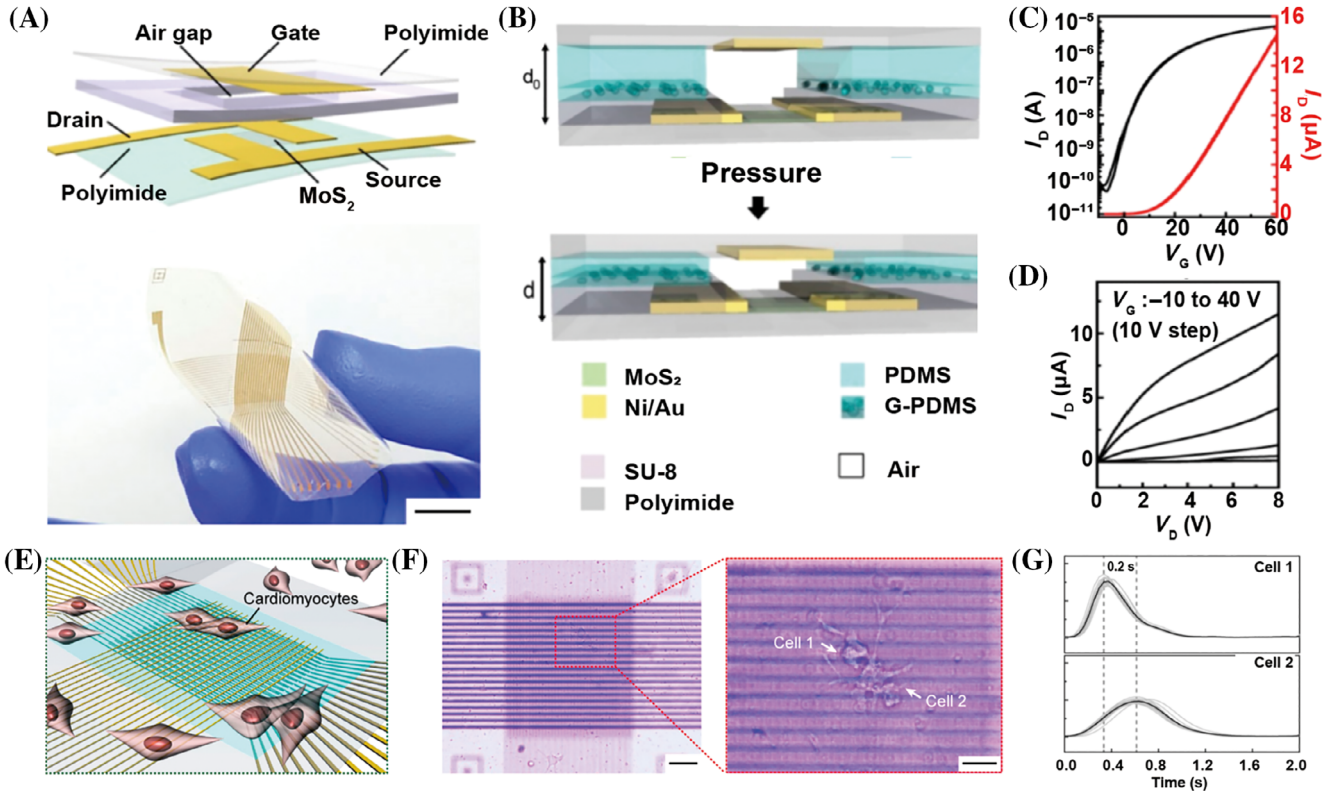

FIGURE 12 (A) Illustration and the photograph of air-dielectric MoS_2 FET, scale bar = 1 cm. (B) MoS_2 FET as a pressure sensor. (C, D) Transfer ($V_D = 1$ V)/output ($V_G = -10$ to 40 V) characteristics of MoS_2 FET. (E) Illustration of MoS_2 FET sensor array for cardiomyocyte pulsation detection. (F) Optical micrographs of MoS_2 FET sensor array, scale bars represent 50 and 20 μm, respectively. (G) The I_D changes of the MoS_2 FET around the cardiomyocytes. Reproduced with permission.[309] Copyright 2020, American Chemical Society. FET, field effect transistor; PDMS, polydimethylsiloxane

transistors can improve their spatial resolution to analyze the pressure distribution in a single cardiomyocyte for precise monitoring (Figure 12E,F). The pressure generated by the cardiomyocyte pulsation changes the I_D of the FET sensor; the pulsation peak and the time to reach the peak of the two cells are also different (Figure 12G). Therefore, this device can measure biological activity even in very small units with excellent resolution, which can facilitate the propagation of cardiomyocyte signals intracellularly and/or intercellularly, which are significantly superior to other pressure sensors.

4 | CONCLUSIONS AND FUTURE PERSPECTIVES

In this review, the physicochemical structures of the most representative emerging 2D materials and the design of their nanostructures for engineering high-performance bioelectronic and biosensing devices are summarized. To guide the future design of bioelectronics, we offer a unique focus on discussing the structural optimization of emerging 2D material-based composites to achieve better performance. Meanwhile, recent developments in emerging 2D materials in bioelectronics, such as neural interface simulation, biomolecular/biomarker detection, and skin sensors, have been introduced in detail. Although the use of emerging 2D materials as bioelectronic devices has been demonstrated in many studies, there is still a long way to go to fill the gap between theoretical research and actual demands.

The first problem to be solved is an optimization of the synthetic process. When designing emerging 2D materials for bioelectronic devices, complex synthetic methods are often introduced during the preparation process. However, these methods may not be controllable when expanding production, which leads to the devices not having ideal structural features or their special surface-related functions being lost, which will become an essential obstacle to the industrialization of bioelectronic devices. At the same time, the stability of the materials prepared by these uncontrollable methods is also worth speculating; when facing a complex environment, it may also lead to the oxidative decomposition of structures and even collapse.

Second, owing to the complex physiological environments, emerging 2D materials that are more suitable for

biological interfaces need to be developed for in vivo biosensing applications. The priority is to ensure their biological safety, and then to maintain stability in long-term contact with tissue interface/body fluid without causing an immune response. This requires a detailed study of the biocompatibility, cytotoxicity, and possible metabolic pathways of the materials. The chemical stability, atomic composition, exfoliation process, and lateral dimensions of emerging 2D materials are the key factors in determining their biocompatibility, whereas PEGylation or functionalization with biocompatible polymers can endow them with enhanced biocompatibility and more favorable profiles on long-term tissue compatibility.[293,310,311] At the same time, the mechanism of electron transfer between biological interfaces and 2D materials should be studied comprehensively. A better understanding of the interaction between 2D materials and various substances can provide more opportunities to explore biosensing applications and improve the current LOD.

Third, each emerging 2D material has unique advantages, but its shortcomings cannot be ignored. Building hybrid nanomaterials with other materials, including and not limited to 2D materials themselves, is an effective way to avoid the original shortcomings. For example, a hybrid of MXene and TMDs has successfully constructed a sensitive and efficient sensor, as shown in Figure 3E. Meanwhile, the mutual hybridization of materials may also bring more interesting material interfaces, which can help to improve their recognition ability and signal amplification while avoiding material defects.

Finally, to realize the joint development of bioelectronics with multiple disciplines, such as materials, medicines, and computational simulation, especially the development of devices integrated with artificial intelligence with the ability to simultaneously detect physical and chemical signals, will be a more comprehensive development direction for the evaluation of human signals by 2D bioelectronic devices. In conclusion, bioelectronic devices obtained by integrating 2D materials with flexible circuit systems can be effectively applied in human body signal detection because of their multifunctional sensing abilities and will be further promoted through the improvement of technology and material performance for high-quality disease monitoring. We believe that with an in-depth understanding of the characteristics and design of emerging 2D materials, as well as new technologies and methods, biocompatible and highly efficient bioelectronics and biosensors can be realized.

ACKNOWLEDGMENTS

This study was financially supported by the National Key R&D Program of China (2021YFE0205000, 2019YFA0110600, and 2019YFA0110601), National Natural Science Foundation of China (Nos. 52173133, 82102064, 82102065, 82071938, 82001824, 82001829, 51903178, and 81971622), the Science and Technology Project of Sichuan Province (Nos. 2021YFH0087, 2021YFH0135, 2021YFS0050, 2021YJ0434, 2021YJ0554, 21YYJC2714, 21ZDYF3763, and 2021YFH0180), China Postdoctoral Science Foundation (2021M692291, 2021M692288, and 2021M702334), the 1·3·5 Project for Disciplines of Excellence, West China Hospital, Sichuan University (No. ZYJC21047), Med-X Center for Materials, Sichuan University (MCM202102), and Fundamental Research Funds for the Central Universities (2021SCU12034 and 2021SCU12013), Post-Doctor Research Project, West China Hospital, Sichuan University (2020HXBH071, 2020HXBH126), and the Science and Technology Project of the Health Planning Committee of Sichuan (20PJ049). Prof. Cheng acknowledges the financial support of the State Key Laboratory of Polymer Materials Engineering (Grant No. sklpme2021-4-02) and Thousand Youth Talents Plan.

CONFLICT OF INTEREST

The authors declare no conflict of interest.

AUTHOR CONTRIBUTIONS

The manuscript was written through the contributions of all authors. All authors have approved the final version of the manuscript.

ORCID

Chong Cheng https://orcid.org/0000-0002-6872-2240

REFERENCES

1. Chen Y, Kim Y-S, Tillman BW, Yeo W-H, Chun Y. Advances in materials for recent low-profile implantable bioelectronics. *Materials*. 2018;11(4):522.
2. He Y, Fan C, Lee S-T. Silicon nanostructures for bioapplications. *Nano Today*. 2010;5(4):282-295.
3. Peng F, Su Y, Zhong Y, Fan C, Lee ST, He Y. Silicon nanomaterials platform for bioimaging, biosensing, and cancer therapy. *Acc Chem Res*. 2014;47(2):612-623.
4. Arshavsky-Graham S, Massad-Ivanir N, Segal E, Weiss S. Porous silicon-based photonic biosensors: current status and emerging applications. *Anal Chem*. 2019;91(1):441-467.
5. Luan E, Shoman H, Ratner DM, Cheung KC, Chrostowski L. Silicon photonic biosensors using label-free detection. *Sensors*. 2018;18(10):3519.
6. Xu Y, Hu X, Kundu S, et al. Silicon-based sensors for biomedical applications: a review. *Sensors*. 2019;19(13):2908.
7. Gao L. Flexible device applications of 2D semiconductors. *Small*. 2017;13(35):1603994.
8. Novoselov KS, Geim AK, Morozov SV, et al. Electric field effect in atomically thin carbon films. *Science*. 2004;306(5696):666-669.
9. Geim AK, Novoselov KS. The rise of graphene. *Nat Mater*. 2007;6(3):183-191.

10. Watanabe K, Taniguchi T, Kanda H. Direct-bandgap properties and evidence for ultraviolet lasing of hexagonal boron nitride single crystal. *Nat Mater*. 2004;3(6):404-409.
11. Zhang X, Xie X, Wang H, Zhang J, Pan B, Xie Y. Enhanced photoresponsive ultrathin graphitic-phase C_3N_4 nanosheets for bioimaging. *J Am Chem Soc*. 2013;135(1):18-21.
12. Li L, Yu Y, Ye G, et al. Black phosphorus field-effect transistors. *Nat Nanotechnol*. 2014;9(5):372-377.
13. Funatsu A, Tateishi H, Hatakeyama K, et al. Synthesis of monolayer platinum nanosheets. *Chem Commun*. 2014; 50(62):8503-8506.
14. Hu Y, Huang Y, Tan C, et al. Two-dimensional transition metal dichalcogenide nanomaterials for biosensing applications. *Mater Chem Front*. 2017;1(1):24-36.
15. Molle A, Goldberger J, Houssa M, Xu Y, Zhang SC, Akinwande D. Buckled two-dimensional Xene sheets. *Nat Mater*. 2017;16(2):163-169.
16. Rodenas T, Luz I, Prieto G, et al. Metal-organic framework nanosheets in polymer composite materials for gas separation. *Nat Mater*. 2015;14(1):48-55.
17. Spitler EL, Dichtel WR. Lewis acid-catalysed formation of two-dimensional phthalocyanine covalent organic frameworks. *Nat Chem*. 2010;2(8):672-677.
18. Yoon J, Lee T, Choi JW. Development of bioelectronic devices using bionanohybrid materials for biocomputation system. *Micromachines*. 2019;10(5):347.
19. Gao D, Parida K, Lee PS. Emerging soft conductors for bioelectronic interfaces. *Adv Funct Mater*. 2020;30(29):1907184.
20. Zhang T, Liu J, Wang C, Leng X, Xiao Y, Fu L. Synthesis of graphene and related two-dimensional materials for bioelectronics devices. *Biosens Bioelectron*. 2017;89(Pt 1):28-42.
21. Huang S, Liu Y, Zhao Y, Ren Z, Guo C. Flexible electronics: stretchable electrodes and their future. *Adv Funct Mater*. 2019;29(6):1805924.
22. Wen W, Song Y, Yan X, et al. Recent advances in emerging 2D nanomaterials for biosensing and bioimaging applications. *Mater Today*. 2018;21(2):164-177.
23. Huh W, Lee D, Lee CH. Memristors based on 2D materials as an artificial synapse for neuromorphic electronics. *Adv Mater*. 2020;32(51):e2002092.
24. Wang B, Sun Y, Ding H, et al. Bioelectronics-related 2D materials beyond graphene: fundamentals, properties, and applications. *Adv Funct Mater*. 2020;30(46):2003732.
25. Bolotsky A, Butler D, Dong C, et al. Two-dimensional materials in biosensing and healthcare: from in vitro diagnostics to optogenetics and beyond. *ACS Nano*. 2019;13(9):9781-9810.
26. Dash M, Chiellini F, Ottenbrite RM, Chiellini E. Chitosan-a versatile semi-synthetic polymer in biomedical applications. *Prog Polym Sci*. 2011;36(8):981-1014.
27. Nicolas J, Mura S, Brambilla D, Mackiewicz N, Couvreur P. Design, functionalization strategies and biomedical applications of targeted biodegradable/biocompatible polymer-based nanocarriers for drug delivery. *Chem Soc Rev*. 2013;42(3):1147-1235.
28. Hu Y, Li Y, Xu F. Versatile functionalization of polysaccharides via polymer grafts: from design to biomedical applications. *Acc Chem Res*. 2017;50(2):281-292.
29. Song Z, Han Z, Lv S, et al. Synthetic polypeptides: from polymer design to supramolecular assembly and biomedical application. *Chem Soc Rev*. 2017;46(21):6570-6599.
30. Liu T, Wang C, Gu X, et al. Drug delivery with PEGylated MoS_2 nano-sheets for combined photothermal and chemotherapy of cancer. *Adv Mater*. 2014;26(21): 3433-3440.
31. Kim JS, Yoo HW, Choi HO, Jung HT. Tunable volatile organic compounds sensor by using thiolated ligand conjugation on MoS_2. *Nano Lett*. 2014;14(10):5941-5947.
32. Qin Z, Ouyang C, Zhang J, et al. 2D WS_2 nanosheets with TiO_2 quantum dots decoration for high-performance ammonia gas sensing at room temperature. *Sens Actuators B*. 2017; 253:1034-1042.
33. Li B, Zu S, Zhang Z, et al. Large Rabi splitting obtained in Ag-WS_2 strong-coupling heterostructure with optical microcavity at room temperature. *Opto-Electronic Adv*. 2019;2(5):190008.
34. Yang G, Gong H, Liu T, Sun X, Cheng L, Liu Z. Two-dimensional magnetic WS_2@Fe_3O_4 nanocomposite with mesoporous silica coating for drug delivery and imaging-guided therapy of cancer. *Biomaterials*. 2015;60:62-71.
35. Kim SJ, Cho KW, Cho HR, et al. Stretchable and transparent biointerface using cell-sheet–graphene hybrid for electrophysiology and therapy of skeletal muscle. *Adv Funct Mater*. 2016; 26(19):3207-3217.
36. Yoo G, Park H, Kim M, et al. Real-time electrical detection of epidermal skin MoS_2 biosensor for point-of-care diagnostics. *Nano Res*. 2016;10(3):767-775.
37. Sangwan VK, Lee H-S, Bergeron H, et al. Multi-terminal memtransistors from polycrystalline monolayer molybdenum disulfide. *Nature*. 2018;554(7693):500-504.
38. Sun L, Zhang Y, Hwang G, et al. Synaptic computation enabled by joule heating of single-layered semiconductors for sound localization. *Nano Lett*. 2018;18(5):3229-3234.
39. Lei Y, Zhao W, Zhang Y, et al. A MXene-based wearable biosensor system for high-performance in vitro perspiration analysis. *Small*. 2019;15(19):1901190.
40. Yang C, Shang D, Liu N, et al. All-solid-state synaptic transistor with ultralow conductance for neuromorphic computing. *Adv Funct Mater*. 2018;28(42):1804170.
41. Wang K, Lou Z, Wang L, et al. Bioinspired interlocked structure-induced high deformability for two-dimensional titanium carbide (MXene)/natural microcapsule-based flexible pressure sensors. *ACS Nano*. 2019;13(8):9139-9147.
42. Zhang YZ, Lee KH, Anjum DH, et al. MXenes stretch hydrogel sensor performance to new limits. *Sci Adv*. 2018;4(6):eaat0098.
43. Li M, Wang B, An X, et al. A practical graphitic carbon nitride (g-C_3N_4) based fluorescence sensor for the competitive detection of trithiocyanuric acid and mercury ions. *Dyes Pigm*. 2019;170:107476.
44. Chen S, Lv Y, Shen Y, et al. Highly sensitive and quality self-testable electrochemiluminescence assay of DNA methyltransferase activity using multifunctional sandwich-assembled carbon nitride nanosheets. *ACS Appl Mater Interfaces*. 2018; 10(8):6887-6894.
45. Tiwari JN, Seo YK, Yoon T, et al. Accelerated bone regeneration by two-photon photoactivated carbon nitride nanosheets. *ACS Nano*. 2017;11(1):742-751.
46. Liu J, Luo Y, Wang Y, et al. Graphitic carbon nitride nanosheets-based ratiometric fluorescent probe forhighly sensitive detection of H_2O_2 and glucose. *ACS Appl Mater Interfaces*. 2016;8(49):33439-33445.

47. Liu M, Zhang H, Zhang X, et al. Nanozyme sensor array plus solvent-mediated signal amplification strategy for ultrasensitive ratiometric fluorescence detection of exosomal proteins and cancer identification. *Anal Chem*. 2021;93(25): 9002-9010.
48. Kathiresan V, Rajarathinam T, Lee S, et al. Cost-effective electrochemical activation of graphitic carbon nitride on the glassy carbon electrode surface for selective determination of serotonin. *Sensors*. 2020;20(21):6083.
49. Guo Z, Li B, Zhang Y, et al. Acid-treated graphitic carbon nitride nanosheets as fluorescence probe for detection of hemin. *ChemistrySelect*. 2019;4(28):8178-8182.
50. Chen Y, Ren R, Pu H, Chang J, Mao S, Chen J. Field-effect transistor biosensors with two-dimensional black phosphorus nanosheets. *Biosens Bioelectron*. 2017;89(Pt 1):505-510.
51. Ahmed T, Kuriakose S, Mayes ELH, et al. Optically stimulated artificial synapse based on layered black phosphorus. *Small*. 2019;15(22):1900966.
52. Kumar V, Brent JR, Shorie M, et al. Nanostructured aptamer-functionalized black phosphorus sensing platform for label-free detection of myoglobin, a cardiovascular disease biomarker. *ACS Appl Mater Interfaces*. 2016;8(35):22860-22868.
53. Hu Z, Li Y, Hussain E, et al. Black phosphorus nanosheets based sensitive protease detection and inhibitor screening. *Talanta*. 2019;197:270-276.
54. Zhou J, Li Z, Ying M, et al. Black phosphorus nanosheets for rapid microRNA detection. *Nanoscale*. 2018;10(11):5060-5064.
55. Park YJ, Sharma BK, Shinde SM, et al. All MoS_2-based large area, skin-attachable active-matrix tactile sensor. *ACS Nano*. 2019;13(3):3023-3030.
56. Park M, Park YJ, Chen X, Park YK, Kim MS, Ahn JH. MoS_2-based tactile sensor for electronic skin applications. *Adv Mater*. 2016;28(13):2556-2562.
57. Govindasamy M, Wang S-F, Jothiramalingam R, Noora Ibrahim S, Al-lohedan HA. A screen-printed electrode modified with tungsten disulfide nanosheets for nanomolar detection of the arsenic drug roxarsone. *Microchim Acta*. 2019; 186(7):420.
58. Loo AH, Bonanni A, Ambrosi A, Pumera M. Molybdenum disulfide (MoS_2) nanoflakes as inherently electroactive labels for DNA hybridization detection. *Nanoscale*. 2014;6(20): 11971-11975.
59. Lee D-W, Lee J, Sohn IY, et al. Field-effect transistor with a chemically synthesized MoS_2 sensing channel for label-free and highly sensitive electrical detection of DNA hybridization. *Nano Res*. 2015;8(7):2340-2350.
60. Wang L, Wang Y, Wong JI, Palacios T, Kong J, Yang HY. Functionalized MoS_2 nanosheet-based field-effect biosensor for label-free sensitive detection of cancer marker proteins in solution. *Small*. 2014;10(6):1101-1105.
61. Sarkar D, Liu W, Xie X, Anselmo AC, Mitragotri S, Banerjee K. MoS_2 field-effect transistor for next-generation label-free biosensors. *ACS Nano*. 2014;8(4):3992-4003.
62. Shan J, Li J, Chu X, et al. High sensitivity glucose detection at extremely low concentrations using a MoS_2-based field-effect transistor. *RSC Adv*. 2018;8(15):7942-7948.
63. Cheng P, Sun K, Hu YH. Memristive behavior and ideal memristor of 1T phase MoS_2 nanosheets. *Nano Lett*. 2016; 16(1):572-576.
64. John RA, Liu F, Chien NA, et al. Synergistic gating of electro-iono-photoactive 2D chalcogenide neuristors: coexistence of hebbian and homeostatic synaptic metaplasticity. *Adv Mater*. 2018;30(25):e1800220.
65. Fathi-Hafshejani P, Azam N, Wang L, et al. Two-dimensional-material-based field-effect transistor biosensor for detecting COVID-19 virus (SARS-CoV-2). *ACS Nano*. 2021;15(7):11461-11469.
66. Yan X, Zhao Q, Chen AP, et al. Vacancy-induced synaptic behavior in 2D WS_2 nanosheet–based memristor for low-power neuromorphic computing. *Small*. 2019;15(24):1901423.
67. Xu B, Zhu M, Zhang W, et al. Ultrathin MXene-micropattern-based field-effect transistor for probing neural activity. *Adv Mater*. 2016;28(17):3333-3339.
68. Zhang H, Wang Z, Zhang Q, Wang F, Liu Y. Ti_3C_2 MXenes nanosheets catalyzed highly efficient electrogenerated chemiluminescence biosensor for the detection of exosomes. *Biosens Bioelectron*. 2019;124-125:184-190.
69. Wu L, Lu X, Dhanjai, et al. 2D transition metal carbide MXene as a robust biosensing platform for enzyme immobilization and ultrasensitive detection of phenol. *Biosens Bioelectron*. 2018;107:69-75.
70. Driscoll N, Richardson AG, Maleski K, et al. Two-dimensional Ti_3C_2 MXene for high-resolution neural interfaces. *ACS Nano*. 2018;12(10):10419-10429.
71. Ma Y, Liu N, Li L, et al. A highly flexible and sensitive piezoresistive sensor based on MXene with greatly changed interlayer distances. *Nat Commun*. 2017;8(1):1207.
72. Sokolov A, Ali M, Li H, Jeon YR, Ko MJ, Choi C. Partially oxidized MXene $Ti_3C_2T_x$ sheets for memristor having synapse and threshold resistive switching characteristics. *Adv Electron Mater*. 2020;7(2):2000866.
73. Wang K, Jia Y, Yan X. Neuro-receptor mediated synapse device based on the crumpled MXene $Ti_3C_2T_x$ nanosheets. *Adv Funct Mater*. 2021;31(48):2104304.
74. Boota M, Anasori B, Voigt C, Zhao MQ, Barsoum MW, Gogotsi Y. Pseudocapacitive electrodes produced by oxidant-free polymerization of pyrrole between the layers of 2D titanium carbide (MXene). *Adv Mater*. 2016;28(7):1517-1522.
75. Ding G, Yang B, Zhou K, et al. Synaptic plasticity and filtering emulated in metal–organic frameworks nanosheets based transistors. *Adv Electron Mater*. 2019;6(1):1900978.
76. Qiao X, Ma X, Ma X, Yue T, Sheng Q. A label-free aptasensor for ochratoxin a detection with signal amplification strategies on ultrathin micron-sized 2D MOF sheets. *Sens Actuators B*. 2021;334:129682.
77. Wang Y, Zhao M, Ping J, et al. Bioinspired design of ultrathin 2D bimetallic metal–organic-framework nanosheets used as biomimetic enzymes. *Adv Mater*. 2016;28(21):4149-4155.
78. Ling W, Hao Y, Wang H, Xu H, Huang X. A novel Cu-metal-organic framework with two-dimensional layered topology for electrochemical detection using flexible sensors. *Nanotechnology*. 2019;30(42):424002.
79. He L, Duan F, Song Y, et al. 2D zirconium-based metal-organic framework nanosheets for highly sensitive detection of mucin 1: consistency between electrochemical and surface plasmon resonance methods. *2D Mater*. 2017;4(2):025098.
80. Li W, Lv S, Wang Y, Zhang L, Cui X. Nanoporous gold induced vertically standing 2D NiCo bimetal-organic

framework nanosheets for non-enzymatic glucose biosensing. *Sens Actuators B*. 2019;281:652-658.
81. Yuan A, Lu Y, Zhang X, Chen Q, Huang Y. Two-dimensional iron MOF nanosheet as a highly efficient nanozyme for glucose biosensing. *J Mater Chem B*. 2020;8(40):9295-9303.
82. Wang X, Xiao S, Jiang Z, et al. An ultrathin 2D Yb(III) metal-organic frameworks with strong electrochemiluminescence as a "on-off-on" platform for detection of picric acid and berberine chloride form. *Talanta*. 2021;234:122625.
83. Fu X, Dong H, Zhen Y, Hu W. Solution-processed large-area nanocrystal arrays of metal–organic frameworks as wearable, ultrasensitive, electronic skin for health monitoring. *Small*. 2015;11(27):3351-3356.
84. Liu Y, Wei Y, Liu M, et al. Two-dimensional metal-organic framework film for realizing optoelectronic synaptic plasticity. *Angew Chem Int Ed*. 2021;60(32):17440-17445.
85. Chen J, Xu Y, Xu F, Zhang Q, Li S, Lu X. Detection of hydrogen peroxide and glucose with a novel fluorescent probe by the enzymatic reaction of amino functionalized MOF nanosheets. *Anal Methods*. 2021;13(37):4228-4237.
86. Yang Y, Hu G, Liang W, et al. An AIEgen-based 2D ultrathin metal–organic layer as an electrochemiluminescence platform for ultrasensitive biosensing of carcinoembryonic antigen. *Nanoscale*. 2020;12(10):5932-5941.
87. Guo C, Li Z, Duan F, Zhang Z, Marchetti F, du M. Semiconducting Cu_xNi_{3-x}(hexahydroxytriphenylene)$_2$ framework for electrochemical aptasensing of C6 glioma cells and epidermal growth factor receptor. *J Mater Chem B*. 2020;8(43):9951-9960.
88. Yan M, Ye J, Zhu Q, Zhu L, Huang J, Yang X. Ultrasensitive immunosensor for cardiac troponin I detection based on the electrochemiluminescence of 2D Ru-MOF nanosheets. *Anal Chem*. 2019;91(15):10156-10163.
89. Wang M, Hu M, Liu J, et al. Covalent organic framework-based electrochemical aptasensors for the ultrasensitive detection of antibiotics. *Biosens Bioelectron*. 2019;132:8-16.
90. Peng Y, Huang Y, Zhu Y, et al. Ultrathin two-dimensional covalent organic framework nanosheets: preparation and application in highly sensitive and selective DNA detection. *J Am Chem Soc*. 2017;139(25):8698-8704.
91. Yan X, Song Y, Liu J, et al. Two-dimensional porphyrin-based covalent organic framework: a novel platform for sensitive epidermal growth factor receptor and living cancer cell detection. *Biosens Bioelectron*. 2019;126:734-742.
92. Li W, Yang C, Yan X. A versatile covalent organic framework-based platform for sensing biomolecules. *Chem Commun*. 2017;53(83):11469-11471.
93. Li T, Yu H, Xiong Z, Gao Z, Zhou Y, Han ST. 2D oriented covalent organic frameworks for alcohol-sensory synapses. *Mater Horiz*. 2021;8(7):2041-2049.
94. Yang C, Shang D, Liu N, et al. A synaptic transistor based on quasi-2D molybdenum oxide. *Adv Mater*. 2017;29(27):1700906.
95. Zhang N, Li K, Zhang T, et al. Electron-rich two-dimensional molybdenum trioxides for highly integrated plasmonic biosensing. *ACS Photonics*. 2018;5(2):347-352.
96. Zhai W, Wang C, Yu P, Wang Y, Mao L. Single-layer MnO_2 nanosheets suppressed fluorescence of 7-hydroxycoumarin: mechanistic study and application for sensitive sensing of ascorbic acid in vivo. *Anal Chem*. 2014;86(24):12206-12213.
97. Fan D, Shang C, Gu W, Wang E, Dong S. Introducing ratiometric fluorescence to MnO_2 nanosheet-based biosensing: a simple, label-free ratiometric fluorescent sensor programmed by cascade logic circuit for ultrasensitive GSH detection. *ACS Appl Mater Interfaces*. 2017;9(31):25870-25877.
98. Ganganboina AB, Dutta Chowdhury A, Doong RA. N-doped graphene quantum dots-decorated V_2O_5 nanosheet for fluorescence turn off-on detection of cysteine. *ACS Appl Mater Interfaces*. 2018;10(1):614-624.
99. Huang C, Chang H, Yang T, et al. Artificial synapse based on a 2D-SnO_2 memtransistor with dynamically tunable analog switching for neuromorphic computing. *ACS Appl Mater Interfaces*. 2021;13(44):52822-52832.
100. Zou J, Wu S, Liu Y, et al. An ultra-sensitive electrochemical sensor based on 2D g-C_3N_4/CuO nanocomposites for dopamine detection. *Carbon*. 2018;130:652-663.
101. Liu P, Huo X, Tang Y, Xu J, Liu X, Wong DKY. A TiO_2 nanosheet-g-C_3N_4 composite photoelectrochemical enzyme biosensor excitable by visible irradiation. *Anal Chim Acta*. 2017;984:86-95.
102. Li Y, Bu Y, Jiang F, Dai X, Ao JP. Fabrication of ultrasensitive photoelectrochemical aptamer biosensor: based on semiconductor/DNA interfacial multifunctional reconciliation via 2D-C_3N_4. *Biosens Bioelectron*. 2020;150:111903.
103. Fu X, Hou F, Liu F, et al. Electrochemiluminescence energy resonance transfer in 2D/2D heterostructured g-C_3N_4/MnO_2 for glutathione detection. *Biosens Bioelectron*. 2019;129:72-78.
104. Hua X, Tian D, Xia F, Zhou C, Wu G. Ultrasensitive electrochemiluminescent immunosensor using MoS_2/g-C_3N_4 nanosheets. *J Electrochem Soc*. 2017;164(9):B456-B462.
105. Li L, Zhao Y, Li X, Ma H, Wei Q. Label-free electrochemiluminescence immunosensor based on Ce-MOF@g-C_3N_4/au nanocomposite for detection of N-terminal pro-B-type natriuretic peptide. *J Electroanal Chem*. 2019;847:113222.
106. Peng J, Lai Y, Chen Y, Xu J, Sun L, Weng J. Sensitive detection of carcinoembryonic antigen using stability-limited few-layer black phosphorus as an electron donor and a reservoir. *Small*. 2017;13(15):1603589.
107. Wang Y, Wu F, Liu X, et al. High on/off ratio black phosphorus based memristor with ultra-thin phosphorus oxide layer. *Appl Phys Lett*. 2019;115(19):193503.
108. Xiong X, Kang J, Hu Q, et al. Reconfigurable logic-in-memory and multilingual artificial synapses based on 2D heterostructures. *Adv Funct Mater*. 2020;30(11):1909645.
109. Huang J, He Y, Jin J, Li Y, Dong Z, Li R. A novel glucose sensor based on MoS_2 nanosheet functionalized with Ni nanoparticles. *Electrochim Acta*. 2014;136:41-46.
110. Liu J, Chen X, Wang Q, et al. Ultrasensitive monolayer MoS_2 field-effect transistor based DNA sensors for screening of down syndrome. *Nano Lett*. 2019;19(3):1437-1444.
111. Shen S, Wang X, Tian Y, et al. Laser-reconfigured MoS_2/ZnO van der Waals synapse. *Nanoscale*. 2019;11(23):11114-11120.
112. He H, Yang R, Huang H, et al. Multi-gate memristive synapses realized with the lateral heterostructure of 2D WSe_2 and WO_3. *Nanoscale*. 2020;12(1):380-387.
113. Huh W, Jang S, Lee JY, et al. Synaptic barristor based on phase-engineered 2D heterostructures. *Adv Mater*. 2018;30(35):e1801447.

114. Yan X, Qin C, Lu C, et al. Robust ag/ZrO_2/WS_2/Pt memristor for neuromorphic computing. *ACS Appl Mater Interfaces*. 2019;11(51):48029-48038.
115. Zhu J, Yang Y, Jia R, et al. Ion gated synaptic transistors based on 2D van der Waals crystals with tunable diffusive dynamics. *Adv Mater*. 2018;30(21):e1800195.
116. Xu R, Jang H, Lee M-H, et al. Vertical MoS_2 double-layer memristor with electrochemical metallization as an atomic-scale synapse with switching thresholds approaching 100 mV. *Nano Lett*. 2019;19(4):2411-2417.
117. Lorencova L, Bertok T, Filip J, et al. Highly stable $Ti_3C_2T_x$ (MXene)/Pt nanoparticles-modified glassy carbon electrode for H_2O_2 and small molecules sensing applications. *Sens Actuators B*. 2018;263:360-368.
118. Rakhi RB, Nayak P, Xia C, Alshareef HN. Novel amperometric glucose biosensor based on MXene nanocomposite. *Sci Rep*. 2016;6(1):36422.
119. Wang F, Yang C, Duan M, Tang Y, Zhu J. TiO_2 nanoparticle modified organ-like Ti_3C_2 MXene nanocomposite encapsulating hemoglobin for a mediator-free biosensor with excellent performances. *Biosens Bioelectron*. 2015;74:1022-1028.
120. Shu Y, Lu Q, Yuan F, et al. Stretchable electrochemical biosensing platform based on Ni-MOF composite/Au nanoparticle-coated carbon nanotubes for real-time monitoring of dopamine released from living cells. *ACS Appl Mater Interfaces*. 2020;12(44):49480-49488.
121. Tan B, Zhao H, Wu W, Liu X, Zhang Y, Quan X. Fe_3O_4-AuNPs anchored 2D metal-organic framework nanosheets with DNA regulated switchable peroxidase-like activity. *Nanoscale*. 2017;9(47):18699-18710.
122. Chen S, Zhao P, Jiang L, et al. Cu_2O-mediated assembly of electrodeposition of au nanoparticles onto 2D metal-organic framework nanosheets for real-time monitoring of hydrogen peroxide released from living cells. *Anal Bioanal Chem*. 2021; 413(2):613-624.
123. Jiang Z, Zhao T, Li C, Li Y, Huang C. 2D MOF-based photoelectrochemical aptasensor for SARS-CoV-2 spike glycoprotein detection. *ACS Appl Mater Interfaces*. 2021;13(42):49754-49761.
124. Ge L, Xu Y, Ding L, You F, Liu Q, Wang K. Perovskite-type $BiFeO_3$/ultrathin graphite-like carbon nitride nanosheets p-n heterojunction: boosted visible-light-driven photoelectrochemical activity for fabricating ampicillin aptasensor. *Biosens Bioelectron*. 2019;124–125:33-39.
125. Malik R, Tomer VK, Dankwort T, Mishra YK, Kienle L. Cubic mesoporous Pd-WO_3 loaded graphitic carbon nitride (g-CN) nanohybrids: highly sensitive and temperature dependent VOC sensors. *J Mater Chem A*. 2018;6(23):10718-10730.
126. Yan J, Rodrigues MTF, Song Z, et al. Reversible formation of g-C_3N_4 3D hydrogels through ionic liquid activation: gelation behavior and room-temperature gas-sensing properties. *Adv Funct Mater*. 2017;27(22):1700653.
127. Liao X, Wang Q, Ju H. Simultaneous sensing of intracellular microRNAs with a multi-functionalized carbon nitride nanosheet probe. *Chem Commun*. 2014;50(88):13604-13607.
128. Xiong M, Rong Q, Meng H, Zhang X. Two-dimensional graphitic carbon nitride nanosheets for biosensing applications. *Biosens Bioelectron*. 2017;89(Pt 1):212-223.
129. Zhou Z, Zhang Y, Shen Y, Liu S, Zhang Y. Molecular engineering of polymeric carbon nitride: advancing applications from photocatalysis to biosensing and more. *Chem Soc Rev*. 2018;47(7):2298-2321.
130. Majdoub M, Anfar Z, Amedlous A. Emerging chemical functionalization of g-C_3N_4: covalent/noncovalent modifications and applications. *ACS Nano*. 2020;14(10):12390-12469.
131. Wu L, Sha Y, Li W, et al. One-step preparation of disposable multi-functionalized g-C_3N_4 based electrochemiluminescence immunosensor for the detection of CA125. *Sens Actuators B*. 2016;226:62-68.
132. Wang Y, Li X, Waterhouse GIN, Zhou Y, Yin H, Ai S. Photoelectrochemical biosensor for protein kinase A detection based on carbon microspheres, peptide functionalized Au-ZIF-8 and TiO_2/g-C_3N_4. *Talanta*. 2019;196:197-203.
133. Giannakoudakis DA, Hu Y, Florent M, Bandosz TJ. Smart textiles of MOF/g-C_3N_4 nanospheres for the rapid detection/detoxification of chemical warfare agents. *Nanoscale Horiz*. 2017;2(6):356-364.
134. Li B, Lai C, Zeng G, et al. Black phosphorus, a rising star 2D nanomaterial in the post-graphene era: synthesis, properties, modifications, and photocatalysis applications. *Small*. 2019; 15(8):1804565.
135. Wu S, Hui KS, Hui KN. 2D black phosphorus: from preparation to applications for electrochemical energy storage. *Adv Sci*. 2018;5(5):1700491.
136. Wang H, Yu X. Few-layered black phosphorus: from fabrication and customization to biomedical applications. *Small*. 2018;14(6):1702830.
137. Luo M, Fan T, Zhou Y, Zhang H, Mei L. 2D black phosphorus–based biomedical applications. *Adv Funct Mater*. 2019;29(13):1808306.
138. Hanlon D, Backes C, Doherty E, et al. Liquid exfoliation of solvent-stabilized few-layer black phosphorus for applications beyond electronics. *Nat Commun*. 2015;6(1):8563.
139. Liu Y, Cai Y, Zhang G, Zhang Y, Ang K. Al-doped black phosphorus p–n homojunction diode for high performance photovoltaic. *Adv Funct Mater*. 2017;27(7):1604638.
140. Maity A, Sui X, Pu H, et al. Sensitive field-effect transistor sensors with atomically thin black phosphorus nanosheets. *Nanoscale*. 2020;12(3):1500-1512.
141. Ryder CR, Wood JD, Wells SA, et al. Covalent functionalization and passivation of exfoliated black phosphorus via aryl diazonium chemistry. *Nat Chem*. 2016;8(6):597-602.
142. Li Q, Zhou Q, Niu X, Zhao Y, Chen Q, Wang J. Covalent functionalization of black phosphorus from first-principles. *J Phys Chem Lett*. 2016;7(22):4540-4546.
143. Abellan G, Lloret V, Mundloch U, et al. Noncovalent functionalization of black phosphorus. *Angew Chem Int Ed*. 2016; 55(47):14557-14562.
144. Sun Z, Xie H, Tang S, et al. Ultrasmall black phosphorus quantum dots: synthesis and use as photothermal agents. *Angew Chem Int Ed*. 2015;54(39):11526-11530.
145. Yi Y, Yu X, Zhou W, Wang J, Chu PK. Two-dimensional black phosphorus: synthesis, modification, properties, and applications. *Mater Sci Eng R*. 2017;120:1-33.
146. Eswaraiah V, Zeng Q, Long Y, Liu Z. Black phosphorus nanosheets: synthesis, characterization and applications. *Small*. 2016;12(26):3480-3502.
147. Cheng J, Gao L, Li T, et al. Two-dimensional black phosphorus nanomaterials: emerging advances in electrochemical energy storage science. *Nano-Micro Lett*. 2020;12(1):179.

148. Liu H, Neal AT, Zhu Z, et al. Phosphorene: an unexplored 2D semiconductor with a high hole mobility. *ACS Nano*. 2014; 8(4):4033-4041.
149. Koenig SP, Doganov RA, Schmidt H, Neto AHC, Ozyilmaz B. Electric field effect in ultrathin black phosphorus. *Appl Phys Lett*. 2014;104(10):103106.
150. Lin Z, Thee MT, Elias AL, et al. Facile synthesis of MoS_2 and $MoXW_{1-x}S_2$ triangular monolayers. *APL Mater*. 2014;2(9): 092514.
151. Brent JR, Savjani N, Lewis EA, Haigh SJ, Lewis DJ, O'Brien P. Production of few-layer phosphorene by liquid exfoliation of black phosphorus. *Chem Commun*. 2014;50(87):13338-13341.
152. Wu L, Guo J, Wang Q, et al. Sensitivity enhancement by using few-layer black phosphorus-graphene/TMDCs heterostructure in surface plasmon resonance biochemical sensor. *Sens Actuators B*. 2017;249:542-548.
153. Pumera M. Phosphorene and black phosphorus for sensing and biosensing. *TrAC Trends Anal Chem*. 2017;93:1-6.
154. Zhuge Z, Tang Y, Tao J, Zhao Y. Functionalized black phosphorus nanocomposite for biosensing. *ChemElectroChem*. 2019;6(4):1129-1133.
155. Zhang T, Wan Y, Xie H, et al. Degradation chemistry and stabilization of exfoliated few-layer black phosphorus in water. *J Am Chem Soc*. 2018;140(24):7561-7567.
156. Liu Y, Chen M, Yang S. Chemical functionalization of 2D black phosphorus. *Inf Dent*. 2021;3(3):231-251.
157. Wood JD, Wells SA, Jariwala D, et al. Effective passivation of exfoliated black phosphorus transistors against ambient degradation. *Nano Lett*. 2014;14(12):6964-6970.
158. Xia K, Jian M, Wang C, et al. Seamless graphene-seal-wrap as a removable protective cover for two-dimensional materials. *ACS Mater Lett*. 2020;2(3):215-219.
159. Zhang J, Chen S, Ma Y, et al. Organosilicon modification to enhance the stability of black phosphorus nanosheets under ambient conditions. *J Mater Chem B*. 2018;6(24):4065-4070.
160. Liu T, Liu Z. 2D MoS_2 nanostructures for biomedical applications. *Adv Healthc Mater*. 2018;7(8):e1701158.
161. Hu H, Zavabeti A, Quan H, et al. Recent advances in two-dimensional transition metal dichalcogenides for biological sensing. *Biosens Bioelectron*. 2019;142:111573.
162. Agarwal V, Chatterjee K. Recent advances in the field of transition metal dichalcogenides for biomedical applications. *Nanoscale*. 2018;10(35):16365-16397.
163. Zhou X, Sun H, Bai X. Two-dimensional transition metal dichalcogenides: synthesis, biomedical applications and biosafety evaluation. *Front Bioeng Biotechnol*. 2020;8(236):236.
164. Manzeli S, Ovchinnikov D, Pasquier D, Yazyev OV, Kis A. 2D transition metal dichalcogenides. *Nat Rev Mater*. 2017;2(8): 17033.
165. Sim DM, Kim M, Yim S, et al. Controlled doping of vacancy-containing few-layer MoS_2 via highly stable thiol-based molecular chemisorption. *ACS Nano*. 2015;9(12):12115-12123.
166. Presolski S, Wang L, Loo AH, et al. Functional nanosheet synthons by covalent modification of transition-metal dichalcogenides. *Chem Mater*. 2017;29(5):2066-2073.
167. Illarionov YY, Banshchikov AG, Polyushkin DK, et al. Ultrathin calcium fluoride insulators for two-dimensional field-effect transistors. *Nat Electron*. 2019;2(6):230-235.
168. Chen WY, Jiang X, Lai S-N, Peroulis D, Stanciu L. Nanohybrids of a MXene and transition metal dichalcogenide for selective detection of volatile organic compounds. *Nat Commun*. 2020;11(1):1302.
169. Koman VB, Liu P, Kozawa D, et al. Colloidal nanoelectronic state machines based on 2D materials for aerosolizable electronics. *Nat Nanotechnol*. 2018;13(9):819-827.
170. Mak KF, Lee C, Hone J, Shan J, Heinz TF. Atomically thin MoS_2: a new direct-gap semiconductor. *Phys Rev Lett*. 2010; 105(13):136805.
171. Nicolosi V, Chhowalla M, Kanatzidis MG, Strano MS, Coleman JN. Liquid exfoliation of layered materials. *Science*. 2013;340(6139):1226419.
172. Zeng Z, Sun T, Zhu J, et al. An effective method for the fabrication of few-layer-thick inorganic nanosheets. *Angew Chem Int Ed*. 2012;51(36):9052-9056.
173. Joensen P, Frindt RF, Morrison SR. Single-layer MoS_2. *Mater Res Bull*. 1986;21(4):457-461.
174. Chou SS, De M, Kim J, et al. Ligand conjugation of chemically exfoliated MoS_2. *J Am Chem Soc*. 2013;135(12): 4584-4587.
175. Li Q, Zhao Y, Ling C, Yuan S, Chen Q, Wang J. Towards a comprehensive understanding of the reaction mechanisms between defective MoS_2 and thiol molecules. *Angew Chem Int Ed*. 2017;56(35):10501-10505.
176. Nguyen EP, Carey BJ, Ou JZ, et al. Electronic tuning of 2D MoS_2 through surface functionalization. *Adv Mater*. 2015; 27(40):6225-6229.
177. Liu T, Wang C, Cui W, et al. Combined photothermal and photodynamic therapy delivered by PEGylated MoS_2 nanosheets. *Nanoscale*. 2014;6(19):11219-11225.
178. Kim J, Kim H, Kim WJ. Single-layered MoS_2-PEI-PEG nanocomposite-mediated gene delivery controlled by photo and redox stimuli. *Small*. 2016;12(9):1184-1192.
179. Voiry D, Goswami A, Kappera R, et al. Covalent functionalization of monolayered transition metal dichalcogenides by phase engineering. *Nat Chem*. 2015;7(1):45-49.
180. Tan C, Yu P, Hu Y, et al. High-yield exfoliation of ultrathin two-dimensional ternary chalcogenide nanosheets for highly sensitive and selective fluorescence DNA sensors. *J Am Chem Soc*. 2015;137(32):10430-10436.
181. Li B, Wang J, Zou H, et al. Low-dimensional transition metal dichalcogenide nanostructures based sensors. *Adv Funct Mater*. 2016;26(39):7034-7056.
182. Kim TH, Kim YH, Park SY, Kim SY, Jang HW. Two-dimensional transition metal disulfides for chemoresistive gas sensing: perspective and challenges. *Chem*. 2017;5(2):15.
183. Radisavljevic B, Radenovic A, Brivio J, Giacometti V, Kis A. Single-layer MoS_2 transistors. *Nat Nanotechnol*. 2011;6(3): 147-150.
184. Ahmed S, Yi J. Two-dimensional transition metal dichalcogenides and their charge carrier mobilities in field-effect transistors. *Nano-Micro Lett*. 2017;9(4):50.
185. Han Y, Huang D, Ma Y, et al. Design of hetero-nanostructures on MoS_2 nanosheets to boost NO_2 room-temperature sensing. *ACS Appl Mater Interfaces*. 2018;10(26):22640-22649.
186. Jiang S, Cheng R, Ng R, Huang Y, Duan X. Highly sensitive detection of mercury(II) ions with few-layer molybdenum disulfide. *Nano Res*. 2015;8(1):257-262.
187. Zheng C, Jin X, Li Y, et al. Sensitive molybdenum disulfide based field effect transistor sensor for real-time monitoring of hydrogen peroxide. *Sci Rep*. 2019;9(1):759.

188. Chen X, Liu C, Mao S. Environmental analysis with 2D transition-metal dichalcogenide-based field-effect transistors. *Nano-Micro Lett*. 2020;12(1):95.
189. Du Y, Neal AT, Zhou H, Ye PD. Transport studies in 2D transition metal dichalcogenides and black phosphorus. *J Phys Condens Matter*. 2016;28(26):263002.
190. Fan Q, Wang L, Xu D, et al. Solution-gated transistors of two-dimensional materials for chemical and biological sensors: status and challenges. *Nanoscale*. 2020;12(21):11364-11394.
191. Sajedi-Moghaddam A, Saievar-Iranizad E, Pumera M. Two-dimensional transition metal dichalcogenide/conducting polymer composites: synthesis and applications. *Nanoscale*. 2017;9(24):8052-8065.
192. Kim Y, Park T, Na J, et al. Layered transition metal dichalcogenide/carbon nanocomposites for electrochemical energy storage and conversion applications. *Nanoscale*. 2020;12(16):8608-8625.
193. Li J, Shi Q, Rohr JA, et al. Flexible 3D porous MoS_2/CNTs architectures with ZT of 0.17 at room temperature for wearable thermoelectric applications. *Adv Funct Mater*. 2020;30(36):2002508.
194. Teo WZ, Chng ELK, Sofer Z, Pumera M. Cytotoxicity of exfoliated transition-metal dichalcogenides (MoS_2, WS_2, and WSe_2) is lower than that of graphene and its analogues. *Chem A Eur J*. 2014;20(31):9627-9632.
195. Latiff NM, Sofer Z, Fisher AC, Pumera M. Cytotoxicity of exfoliated layered vanadium dichalcogenides. *Chem A Eur J*. 2017;23(3):684-690.
196. Chia HL, Latiff NM, Sofer Z, Pumera M. Cytotoxicity of group 5 transition metal ditellurides (MTe_2; M=V, Nb, Ta). *Chem A Eur J*. 2018;24(1):206-211.
197. Naguib M, Mochalin VN, Barsoum MW, Gogotsi Y. 25th anniversary article: MXenes: a new family of two-dimensional materials. *Adv Mater*. 2014;26(7):992-1005.
198. Anasori B, Xie Y, Beidaghi M, et al. Two-dimensional, ordered, double transition metals carbides (MXenes). *ACS Nano*. 2015;9(10):9507-9516.
199. Ghidiu M, Kota S, Drozd V, Barsoum MW. Pressure-induced shear and interlayer expansion in Ti_3C_2 MXene in the presence of water. *Sci Adv*. 2018;4(1):eaao6850.
200. Lin H, Gao S, Dai C, Chen Y, Shi J. A two-dimensional biodegradable niobium carbide (MXene) for photothermal tumor eradication in NIR-I and NIR-II biowindows. *J Am Chem Soc*. 2017;139(45):16235-16247.
201. Naguib M, Kurtoglu M, Presser V, et al. Two-dimensional nanocrystals produced by exfoliation of Ti_3AlC_2. *Adv Mater*. 2011;23(37):4248-4253.
202. Qin T, Wang Z, Wang Y, Besenbacher F, Otyepka M, Dong M. Recent progress in emerging two-dimensional transition metal carbides. *Nano-Micro Lett*. 2021;13(1):183.
203. Garg R, Agarwal A, Agarwal M. A review on MXene for energy storage application: effect of interlayer distance. *Mater Res Express*. 2020;7(2):022001.
204. Wang X, Kajiyama S, Iinuma H, et al. Pseudocapacitance of MXene nanosheets for high-power sodium-ion hybrid capacitors. *Nat Commun*. 2015;6(1):6544.
205. Hu YJ, Zhuo H, Luo Q, et al. Biomass polymer-assisted fabrication of aerogels from MXenes with ultrahigh compression elasticity and pressure sensitivity. *J Mater Chem A*. 2019;7(17):10273-10281.
206. Hu M, Hu T, Li Z, et al. Surface functional groups and interlayer water determine the electrochemical capacitance of $Ti_3C_2T_x$ MXene. *ACS Nano*. 2018;12(4):3578-3586.
207. Li H, Du Z. Preparation of a highly sensitive and stretchable strain sensor of MXene/silver nanocomposite-based yarn and wearable applications. *ACS Appl Mater Interfaces*. 2019;11(49):45930-45938.
208. Luo J, Zhang W, Yuan H, et al. Pillared structure design of MXene with ultralarge interlayer spacing for high-performance lithium-ion capacitors. *ACS Nano*. 2017;11(3):2459-2469.
209. Li Z, Zhang H, Han J, Chen Y, Lin H, Yang T. Surface nanopore engineering of 2D MXenes for targeted and synergistic multitherapies of hepatocellular carcinoma. *Adv Mater*. 2018;30(25):e1706981.
210. Xie X, Zhang N. Positioning MXenes in the photocatalysis landscape: competitiveness, challenges, and future perspectives. *Adv Funct Mater*. 2020;30(36):2002528.
211. Du C, Sun X, Yu H, et al. $V_4C_3T_x$ MXene: a promising active substrate for reactive surface modification and the enhanced electrocatalytic oxygen evolution activity. *InfoMat*. 2020;2(5):950-959.
212. Pang J, Mendes RG, Bachmatiuk A, et al. Applications of 2D MXenes in energy conversion and storage systems. *Chem Soc Rev*. 2019;48(1):72-133.
213. Hu M, Zhang H, Hu T, Fan B, Wang X, Li Z. Emerging 2D MXenes for supercapacitors: status, challenges and prospects. *Chem Soc Rev*. 2020;49(18):6666-6693.
214. Iqbal A, Sambyal P, Koo CM. 2D MXenes for electromagnetic shielding: a review. *Adv Funct Mater*. 2020;30(47):2000883.
215. Sinha A, Dhanjai ZHM, et al. MXene: an emerging material for sensing and biosensing. *TrAC Trends Anal Chem*. 2018;105:424-435.
216. Zhang Q, He J, Fu X, et al. Fluorine-free strategy for hydroxylated Ti_3C_2/Ti_3AlC_2 catalysts with enhanced aerobic oxidative desulfurization and mechanism. *Chem Eng J*. 2022;430:132950.
217. Li T, Yao L, Liu Q, et al. Fluorine-free synthesis of high-purity $Ti_3C_2T_x$ (T=OH, O) via alkali treatment. *Angew Chem Int Ed*. 2018;57(21):6115-6119.
218. Sun W, Shah SA, Chen Y, et al. Electrochemical etching of Ti_2AlC to Ti_2CT_x (MXene) in low-concentration hydrochloric acid solution. *J Mater Chem A*. 2017;5(41):21663-21668.
219. Song M, Pang S-Y, Guo F, Wong M-C, Hao J. Fluoride-free 2D niobium carbide MXenes as stable and biocompatible nanoplatforms for electrochemical biosensors with ultrahigh sensitivity. *Adv Sci*. 2020;7(24):2001546.
220. Rafieerad A, Amiri A, Sequiera GL, et al. Development of fluorine-free tantalum carbide MXene hybrid structure as a biocompatible material for supercapacitor electrodes. *Adv Funct Mater*. 2021;31(30):2100015.
221. Yang S, Zhang P, Wang F, et al. Fluoride-free synthesis of two-dimensional titanium carbide (MXene) using a binary aqueous system. *Angew Chem Int Ed*. 2018;57(47):15491-15495.
222. Shen M, Jiang W, Liang K, et al. One-pot green process to synthesize MXene with controllable surface terminations using molten salts. *Angew Chem Int Ed*. 2021;60(52):27013-27018.
223. Bai Y, Liu C, Chen T, et al. MXene-copper/cobalt hybrids via Lewis acidic molten salts etching for high performance symmetric supercapacitor. *Angew Chem Int Ed*. 2021;60(133):25318-25322.

224. Lim GP, Soon CF, Ma NL, et al. Cytotoxicity of MXene-based nanomaterials for biomedical applications: a mini review. *Environ Res*. 2021;201:111592.
225. Szuplewska A, Kulpińska D, Dybko A, et al. Future applications of MXenes in biotechnology, nanomedicine, and sensors. *Trends Biotechnol*. 2020;38(3):264-279.
226. Lin X, Li Z, Qiu J, et al. Fascinating MXene nanomaterials: emerging opportunities in the biomedical field. *Biomater Sci*. 2021;9(16):5437-5471.
227. Li H, Eddaoudi M, O'Keeffe M, Yaghi OM. Design and synthesis of an exceptionally stable and highly porous metal-organic framework. *Nature*. 1999;402(6759):276-279.
228. Furukawa H, Cordova KE, O'Keeffe M, Yaghi OM. The chemistry and applications of metal-organic frameworks. *Science*. 2013;341(6149):1230444.
229. Xuan W, Zhu C, Liu Y, Cui Y. Mesoporous metal-organic framework materials. *Chem Soc Rev*. 2012;41(5):1677-1695.
230. Zheng S, Sun Y, Xue H, et al. Dual-ligand and hard-soft-acid-base strategies to optimize metal-organic framework nanocrystals for stable electrochemical cycling performance. *Natl Sci Rev*. 2021. https://doi.org/10.1093/nsr/nwab197
231. Peng Y, Li Y, Ban Y, et al. Membranes. Metal-organic framework nanosheets as building blocks for molecular sieving membranes. *Science*. 2014;346(6215):1356-1359.
232. Ding Y, Chen Y, Zhang X, et al. Controlled intercalation and chemical exfoliation of layered metal–organic frameworks using a chemically labile intercalating agent. *J Am Chem Soc*. 2017;139(27):9136-9139.
233. Zhao M, Wang Y, Ma Q, et al. Ultrathin 2D metal–organic framework nanosheets. *Adv Mater*. 2015;27(45):7372-7378.
234. Campbell MG, Liu SF, Swager TM, Dinca M. Chemiresistive sensor arrays from conductive 2D metal–organic frameworks. *J Am Chem Soc*. 2015;137(43):13780-13783.
235. Wu G, Huang J, Zang Y, He J, Xu G. Porous field-effect transistors based on a semiconductive metal–organic framework. *J Am Chem Soc*. 2017;139(4):1360-1363.
236. Kamakura Y, Chinapang P, Masaoka S, et al. Semiconductive nature of lead-based metal–organic frameworks with three-dimensionally extended sulfur secondary building units. *J Am Chem Soc*. 2020;142(1):27-32.
237. Gu Z, Chen S, Fu W, Zheng Q, Zhang J. Epitaxial growth of MOF thin film for modifying the dielectric layer in organic field-effect transistors. *ACS Appl Mater Interfaces*. 2017;9(8):7259-7264.
238. Medina DD, Petrus ML, Jumabekov AN, et al. Directional charge-carrier transport in oriented benzodithiophene covalent organic framework thin films. *ACS Nano*. 2017;11(3):2706-2713.
239. Yang T, Song T, Callsen M, et al. Atomically thin 2D transition metal oxides: structural reconstruction, interaction with substrates, and potential applications. *Adv Mater Interfaces*. 2019;6(1):1801160.
240. Wang Y, Zhang S, Haque E, et al. Immobilisation of microperoxidase-11 into layered MoO_3 for applications of enzymatic conversion. *Appl Mater Today*. 2019;16:185-192.
241. Campbell MG, Sheberla D, Liu SF, Swager TM, Dinca M. Cu(3)(hexaiminotriphenylene)(2): an electrically conductive 2D metal-organic framework for chemiresistive sensing. *Angew Chem Int Ed*. 2015;54(14):4349-4352.
242. Evans AM, Parent LR, Flanders NC, et al. Seeded growth of single-crystal two-dimensional covalent organic frameworks. *Science*. 2018;361(6397):52-57.
243. Feng X, Ding X, Jiang D. Covalent organic frameworks. *Chem Soc Rev*. 2012;41(18):6010-6022.
244. Wu X, Han X, Xu Q, et al. Chiral BINOL-based covalent organic frameworks for enantioselective sensing. *J Am Chem Soc*. 2019;141(17):7081-7089.
245. Feldblyum JI, McCreery CH, Andrews SC, et al. Few-layer, large-area, 2D covalent organic framework semiconductor thin films. *Chem Commun*. 2015;51(73):13894-13897.
246. Yang F, Cheng S, Zhang X, et al. 2D organic materials for optoelectronic applications. *Adv Mater*. 2018;30(2):1702415.
247. Liu X, Hu M, Wang M, et al. Novel nanoarchitecture of co-MOF-on-TPN-COF hybrid: Ultralowly sensitive bioplatform of electrochemical aptasensor toward ampicillin. *Biosens Bioelectron*. 2019;123:59-68.
248. Luo Z, Fan S, Gu C, et al. Metal–organic framework (MOF)-based nanomaterials for biomedical applications. *Curr Med Chem*. 2019;26(18):3341-3369.
249. Wu M, Yang Y. Metal–organic framework (MOF)-based drug/cargo delivery and cancer therapy. *Adv Mater*. 2017;29(23):1606134.
250. Zhao F, Liu H, Mathe SDR, Dong A, Zhang J. Covalent organic frameworks: from materials design to biomedical application. *Nanomaterials*. 2018;8(1):15.
251. Liao C, Liu S. Tuning the physicochemical properties of reticular covalent organic frameworks (COFs) for biomedical applications. *J Mater Chem B*. 2021;9(31):6116-6128.
252. Sun F, Li Q, Bai Y, et al. A controllable preparation of two-dimensional cobalt oxalate-based nanostructured sheets for electrochemical energy storage. *Chin Chem Lett*. 2021. https://doi.org/10.1016/j.cclet.2021.10.075
253. Sun Z, Liao T, Dou Y, et al. Generalized self-assembly of scalable two-dimensional transition metal oxide nanosheets. *Nat Commun*. 2014;5(1):3813.
254. Yoon JW, Lee JH. Toward breath analysis on a chip for disease diagnosis using semiconductor-based chemiresistors: recent progress and future perspectives. *Lab Chip*. 2017;17(21):3537-3557.
255. Yang C, Xiao F, Wang J, Su X. 3D flower- and 2D sheet-like CuO nanostructures: microwave-assisted synthesis and application in gas sensors. *Sens Actuators B*. 2015;207:177-185.
256. Dral AP, ten Elshof JE. 2D metal oxide nanoflakes for sensing applications: review and perspective. *Sens Actuators B*. 2018;272:369-392.
257. Miao J, Chen C, Meng L, Lin Y. Self-assembled monolayer of metal oxide nanosheet and structure and gas-sensing property relationship. *ACS Sens*. 2019;4(5):1279-1290.
258. Yin Z, Tordjman M, Lee Y, Vardi A, Kalish R, Alamo JA del. Enhanced transport in transistor by tuning transition-metal oxide electronic states interfaced with diamond. *Sci Adv*. 2018;4(9):eaau0480.
259. Addou R, Dahal A, Batzill M. Growth of a two-dimensional dielectric monolayer on quasi-freestanding graphene. *Nat Nanotechnol*. 2013;8(1):41-45.
260. Tusche C, Meyerheim HL, Kirschner J. Observation of depolarized ZnO(0001) monolayers: formation of unreconstructed planar sheets. *Phys Rev Lett*. 2007;99(2):026102.
261. Hwang HY, Iwasa Y, Kawasaki M, Keimer B, Nagaosa N, Tokura Y. Emergent phenomena at oxide interfaces. *Nat Mater*. 2012;11(2):103-113.
262. Ren B, Wang Y, Ou J. Engineering two-dimensional metal oxides via surface functionalization for biological applications. *J Mater Chem B*. 2020;8(6):1108-1127.

263. Fairfield JA. Nanostructured materials for neural electrical interfaces. *Adv Funct Mater*. 2018;28(12):1701145.
264. Won SM, Song E, Zhao J, Li J, Rivnay J, Rogers JA. Recent advances in materials, devices, and systems for neural interfaces. *Adv Mater*. 2018;30(30):e1800534.
265. Kostarelos K, Vincent M, Hebert C, Garrido JA. Graphene in the design and engineering of next-generation neural interfaces. *Adv Mater*. 2017;29(42):1700909.
266. Wang M, Mi G, Shi D, Bassous N, Hickey D, Webster TJ. Nanotechnology and nanomaterials for improving neural interfaces. *Adv Funct Mater*. 2018;28(12):1700905.
267. Park D-W, Schendel AA, Mikael S, et al. Graphene-based carbon-layered electrode array technology for neural imaging and optogenetic applications. *Nat Commun*. 2014;5(1):5258.
268. Lanche R, Pachauri V, Koppenhofer D, Wagner P, Ingebrandt S. Reduced graphene oxide-based sensing platform for electric cell-substrate impedance sensing. *Phys Status Solidi A*. 2014; 211(6):1404-1409.
269. Hess LH, Seifert M, Garrido JA. Graphene transistors for bioelectronics. *Proc IEEE*. 2013;101(7):1780-1792.
270. Deng M, Yang X, Silke M, et al. Electrochemical deposition of polypyrrole/graphene oxide composite on microelectrodes towards tuning the electrochemical properties of neural probes. *Sens Actuators B*. 2011;158(1):176-184.
271. Chiu CW, He X, Liang H. Surface modification of a neural sensor using graphene. *Electrochim Acta*. 2013;94:42-48.
272. Du X, Wu L, Cheng J, et al. Graphene microelectrode arrays for neural activity detection. *J Biol Phys*. 2015;41(4):339-347.
273. Cheng J, Wu L, Du X, et al. Flexible solution-gated graphene field effect transistor for electrophysiological recording. *J Microelectromech Syst*. 2014;23(6):1311-1317.
274. Li W, Li F, Li H, et al. Flexible circuits and soft actuators by printing assembly of graphene. *ACS Appl Mater Interfaces*. 2016;8(19):12369-12376.
275. Chen CH, Lin CT, Hsu WL, et al. A flexible hydrophilic-modified graphene microprobe for neural and cardiac recording. *Nanomedicine*. 2013;9(5):600-604.
276. Heo C, Yoo J, Lee S, et al. The control of neural cell-to-cell interactions through non-contact electrical field stimulation using graphene electrodes. *Biomaterials*. 2011;32(1):19-27.
277. Tian H, Mi W, Zhao H, et al. A novel artificial synapse with dual modes using bilayer graphene as the bottom electrode. *Nanoscale*. 2017;9(27):9275-9283.
278. Huang W, Xia X, Zhu C, et al. Memristive artificial synapses for neuromorphic computing. *Nano-Micro Lett*. 2021;13(1):85.
279. Kim S, Choi B, Lim M, et al. Pattern recognition using carbon nanotube synaptic transistors with an adjustable weight update protocol. *ACS Nano*. 2017;11(3):2814-2822.
280. Zhu Y, Liu G, Xin Z, Fu C, Wan Q, Shan F. Solution-processed, electrolyte-gated In_2O_3 flexible synaptic transistors for brain-inspired neuromorphic applications. *ACS Appl Mater Interfaces*. 2020;12(1):1061-1068.
281. Luo Z, Xia X, Yang M, et al. Artificial optoelectronic synapses based on ferroelectric field-effect enabled 2D transition metal dichalcogenide memristive transistors. *ACS Nano*. 2020;14(1): 746-754.
282. Cho SW, Kwon SM, Lee M, et al. Multi-spectral gate-triggered heterogeneous photonic neuro-transistors for power-efficient brain-inspired neuromorphic computing. *Nano Energy*. 2019; 66:104097.
283. Sanchez Esqueda I, Yan X, Rutherglen C, et al. Aligned carbon nanotube synaptic transistors for large-scale neuromorphic computing. *ACS Nano*. 2018;12(7):7352-7361.
284. Hafsi B, Boubaker A, Guerin D, et al. Electron-transport polymeric gold nanoparticles memory device, artificial synapse for neuromorphic applications. *Org Electron*. 2017;50:499-506.
285. Han H, Xu Z, Guo K, et al. Tunable synaptic plasticity in crystallized conjugated polymer nanowire artificial synapses. *Adv Intelligent Syst*. 2020;2(3):1900176.
286. Ge C, Liu C, Zhou Q, et al. A ferrite synaptic transistor with topotactic transformation. *Adv Mater*. 2019;31(19):e1900379.
287. Yu F, Zhu L, Gao W, et al. Chitosan-based polysaccharide-gated flexible indium tin oxide synaptic transistor with learning abilities. *ACS Appl Mater Interfaces*. 2018;10(19):16881-16886.
288. Wang S, Chen C, Yu Z, et al. A MoS_2/PTCDA hybrid heterojunction synapse with efficient photoelectric dual modulation and versatility. *Adv Mater*. 2019;31(3):e1806227.
289. Yang Y, Gao W. Wearable and flexible electronics for continuous molecular monitoring. *Chem Soc Rev*. 2019;48(6):1465-1491.
290. Wang P, Peng Z, Li M, Wang Y. Stretchable transparent conductive films from long carbon nanotube metals. *Small*. 2018; 14(38):e1802625.
291. Rogers JA, Lagally MG, Nuzzo RG. Synthesis, assembly and applications of semiconductor nanomembranes. *Nature*. 2011; 477(7362):45-53.
292. Ma Y, Ajayan PM, Yang S, Gong Y. Recent advances in synthesis and applications of 2D junctions. *Small*. 2018;14(38):e1801606.
293. Ge X, Xia Z, Guo S. Recent advances on black phosphorus for biomedicine and biosensing. *Adv Funct Mater*. 2019;29(29): 1900318.
294. Motaghed Mazhabi R, Ge L, Jiang H, Wang X. A facile photoelectrochemical sensor for high sensitive ROS and AA detection based on graphitic carbon nitride nanosheets. *Biosens Bioelectron*. 2018;107:54-61.
295. Du H, Zhang X, Liu Z, Qu F. A supersensitive biosensor based on MoS_2 nanosheet arrays for the real-time detection of H_2O_2 secreted from living cells. *Chem Commun*. 2019;55(65):9653-9656.
296. Kumar S, Lei Y, Alshareef NH, Quevedo-Lopez MA, Salama KN. Biofunctionalized two-dimensional Ti_3C_2 MXenes for ultrasensitive detection of cancer biomarker. *Biosens Bioelectron*. 2018;121:243-249.
297. You I, Choi SE, Hwang H, Han SW, Kim JW, Jeong U. E-skin tactile sensor matrix pixelated by position-registered conductive microparticles creating pressure-sensitive selectors. *Adv Funct Mater*. 2018;28(31):1801858.
298. Wang C, Xia K, Zhang M, Jian M, Zhang Y. An all-silk-derived dual-mode e-skin for simultaneous temperature–pressure detection. *ACS Appl Mater Interfaces*. 2017;9(45): 39484-39492.
299. Chen D, Pei Q. Electronic muscles and skins: a review of soft sensors and actuators. *Chem Rev*. 2017;117(17):11239-11268.
300. Yang H, Xue T, Li F, Liu W, Song Y. Graphene: diversified flexible 2D material for wearable vital signs monitoring. *Adv Mater Technol*. 2019;4(2):1800574.
301. Li T, Li Y, Zhang T. Materials, structures, and functions for flexible and stretchable biomimetic sensors. *Acc Chem Res*. 2019;52(2):288-296.
302. Yasaei P, Behranginia A, Foroozan T, et al. Stable and selective humidity sensing using stacked black phosphorus flakes. *ACS Nano*. 2015;9(10):9898-9905.

303. Choi C, Lee Y, Cho KW, Koo JH, Kim DH. Wearable and implantable soft bioelectronics using two-dimensional materials. *Acc Chem Res*. 2019;52(1):73-81.
304. Guo H, Lan C, Zhou Z, Sun P, Wei D, Li C. Transparent, flexible, and stretchable WS_2 based humidity sensors for electronic skin. *Nanoscale*. 2017;9(19):6246-6253.
305. Li S, Zhang Y, Wang Y, et al. Physical sensors for skin-inspired electronics. *InfoMat*. 2020;2(1):184-211.
306. Wang L, Chen D, Jiang K, Shen G. New insights and perspectives into biological materials for flexible electronics. *Chem Soc Rev*. 2017;46(22):6764-6815.
307. Khan U, Kim TH, Ryu H, Seung W, Kim SW. Graphene tribotronics for electronic skin and touch screen applications. *Adv Mater*. 2017;29(1):1603544.
308. Chen Z, Hu Y, Zhuo H, et al. Compressible, elastic, and pressure-sensitive carbon aerogels derived from 2D titanium carbide nanosheets and bacterial cellulose for wearable sensors. *Chem Mater*. 2019;31(9):3301-3312.
309. Jang J, Kim H, Ji S, et al. Mechanoluminescent, air-dielectric MoS_2 transistors as active-matrix pressure sensors for wide detection ranges from footsteps to cellular motions. *Nano Lett*. 2020;20(1):66-74.
310. Kurapati R, Kostarelos K, Prato M, Bianco A. Biomedical uses for 2D materials beyond graphene: current advances and challenges ahead. *Adv Mater*. 2016;28(29):6052-6074.
311. Wang S, Zhou L, Zheng Y, et al. Synthesis and biocompatibility of two-dimensional biomaterials. *Colloids Surf A*. 2019;583:124004.

AUTHOR BIOGRAPHIES

Sujiao Cao is a post doctoral research fellow at West China Hospital, Sichuan University. She received her Master's degree and PhD degree from South China University of Technology and Sichuan University, respectively. Her current research focuses on synthesizing metal-organic precursors-derived porous carbon for diverse electrocatalysts and biocatalysts.

Lang Ma is now an associate professor at West China Hospital, Sichuan University. He obtained his BS and PhD degrees from Sichuan University, China, in 2012 and 2016, respectively. His current research interests include the design and fabrication of biopolymers functionalized nanomedical materials, nanocatalytic biomaterials, and cellular-mimetic nanomedicines, and their applications in diagnosis and therapies for the biomedical field, such as wound healing, skin tumor, rheumatoid arthritis, and stem cells regenerations.

Chong Cheng is currently a full professor in the department of polymer science at Sichuan University. He obtained his BSc and PhD from Sichuan University. After a research stay at the University of Michigan, Ann Arbor, USA, he joined the Freie Universität Berlin as an AvH research fellow. His current scientific interests include fabricating advanced low-dimensional materials for nanomedicines, antibacterial materials, stem cell scaffolds, energy storage devices, and electrocatalysts, especially the cutting-edge catalytic applications of metal-organic frameworks. He has published over 110 SCI papers, including *Nature Materials*, *Nature Communications*, *Science Advances*, and *Advanced Materials*.

How to cite this article: Chen F, Tang Q, Ma T, et al. Structures, properties, and challenges of emerging 2D materials in bioelectronics and biosensors. *InfoMat*. 2022;4(5):e12299. doi:10.1002/inf2.12299